

Review

Symmetry Restoration and Breaking at Finite Temperature: An Introductory Review

Eibun Senaha ^{1,2} 

¹ Theoretical Particle Physics and Cosmology Research Group, Advanced Institute of Materials Science, Ton Duc Thang University, Ho Chi Minh City 700000, Vietnam; eibun.senaha@tdtu.edu.vn

² Faculty of Applied Sciences, Ton Duc Thang University, Ho Chi Minh City 700000, Vietnam

Received: 30 March 2020; Accepted: 17 April 2020; Published: 5 May 2020



Abstract: Symmetries at finite temperature are of great importance to understand dynamics of spontaneous symmetry breaking phenomena, especially phase transitions in early Universe. Some symmetries such as the electroweak symmetry can be restored in hot environment. However, it is a nontrivial question that the phase transition occurs via first or second order, or even smooth crossover, which strongly depends on underlying physics. If it is first order, gravitational waves can be generated, providing a detectable signal of this epoch. Moreover, the baryon asymmetry of the Universe can also arise under some conditions. In this article, the electroweak phase transition is reviewed, focusing particularly on the case of the first-order phase transition. Much attention is paid to multi-step phase transitions in which additional symmetry breaking such as a spontaneous Z_2 breaking plays a pivotal role in broadening the possibility of the first-order electroweak phase transition. On the technical side, we review thermal resummation that mitigates a bad infrared behavior related to the symmetry restoration. In addition, gauge and scheme dependences of perturbative calculations are also briefly discussed.

Keywords: symmetry restoration and breaking; electroweak phase transition; thermal resummation

1. Introduction

Symmetry and its breaking are key concepts in particle physics and cosmology. The former provides foundation of underlying theories while the latter is often indispensable to describes diversity in nature. Those two conflicting notions are well accommodated in the framework of spontaneous symmetry breaking (SSB), i.e., symmetry is respected by action but broken by vacuum. In this phenomenon, dynamical evolution of the vacuum is of great importance, and in a hot environment the symmetry can be fully restored [1–5].

One of the most intriguing SSB in cosmology is phase transitions at early Universe such as the quantum chromodynamics (QCD) transition and electroweak phase transition (EWPT). Much attention has been given to the latter since the baryon asymmetry of the Universe (BAU) [6], which cannot be realized in the standard model (SM) of particle physics, could arise if EWPT is first order with expanding bubble walls (referred to as electroweak baryogenesis (EWBG) [7], for reviews, see Refs. [8–16]). Moreover, in such a case, gravitational waves can be produced by bubble collisions, turbulence and sound waves, which could be probed by near future experiments such as LISA and DECIGO (for detailed discussion, see, e.g., Ref. [17]). From this point of view, the investigation of the first-order phase transitions, especially EWPT is not only important but urgent in terms of the timeline.

EWPT can be first-order once the SM is extended, for instance, real scalar extensions [18–58], complex scalar extensions [59–69], Higgs doublet extensions [70–88], and supersymmetric extensions [89–107]. As first stressed in Ref. [97], additional symmetry breaking prior to EWPT can broaden the possibility of the first-order EWPT. In the paper, various multi-step phase transitions

are classified in the next-to-minimal supersymmetric SM, and it is shown that a global $U(1)$ breaking induced by a gauge singlet scalar preceding EWPT can help to achieve the first-order EWPT. Currently, this mechanism is widely applied to a plethora of models beyond the SM. One of the simplest models is a real scalar extension of the SM with a Z_2 symmetry. The most attractive 2-step phase transition scenario is that the broken Z_2 symmetry by the first step transition is restored by the second step transition, accommodating both the first-order EWPT and dark matter (DM) candidate simultaneously.

On the technical side in perturbation theories, one is faced with some thorny problems, such as thermal resummation and gauge dependences. It is widely studied that the symmetry restoration brings about infrared divergences that spoil the validity of perturbative expansion at high temperature even though couplings in theories are sufficiently small [3,108]. A standard prescription is called thermal resummation in which perturbative expansion is re-organized in such a way that dominant temperature corrections are summed over and absorbed into zeroth-order terms. In addition to this problem, ordinary perturbative calculations of EWPT are plagued by a gauge dependence problem, which is attributed to the gauge-dependent order parameter, viz, the Higgs vacuum expectation value (VEV). Thus, obtained results such as a critical temperature and strength of the first-order phase transition suffer from the gauge dependence.

In this article, we give some basics for analysis of the thermal phase transitions including thermal resummation in a pedagogical way. Great emphasis is put on EWPT, focusing on multi-step types that pave the way for first-order phase transition as mentioned above. We also cover a recently proposed gauge-invariant treatment of EWPT based on Nielsen-Fukuda-Kugo (NFK) identity [109,110] and its comparisons with gauge-dependent results. Scheme dependences of various calculations are also discussed based on Ref. [56].

The article is organized as follows. In Section 2, we start by giving a finite-temperature effective potential and demonstrate the symmetry restoration in the ϕ^4 theory. In Section 3, after showing the breakdown of the perturbative expansion at high temperature in great detail, its prescription is presented. In Section 4, EWPTs in the SM and its extension by the real scalar are discussed. We also show a gauge-invariant perturbative treatment and make a comparison among different calculations. Summary and outlook are given in Section 5. Some details are relegated to Appendix A. Throughout this article, we exclusively consider flat spacetime and use convention of $g_{\mu\nu} = g^{\mu\nu} = \text{diag}(1, -1, -1, -1)$ in Minkowski space.

2. Symmetry Restoration and Order of Phase Transitions

We start by giving necessary tools for analyzing phase transition at finite temperature. The most basic quantity is partition function, which is defined as [3]

$$Z[T] = \text{Tr}[e^{-H/T}] = N \int_{\text{b.c.}} [d\Psi] \exp \left[- \int_0^{1/T} d\tau \int d^3x \mathcal{L}(\Psi) \right], \quad (1)$$

with the boundary conditions $\phi(0, \mathbf{x}) = \phi(1/T, \mathbf{x})$ for bosons and $\psi(0, \mathbf{x}) = -\psi(1/T, \mathbf{x})$ for fermions, which follow from the property of the traceness of $Z[T]$. Because of this boundary conditions, Fourier modes of the imaginary time τ are discretized (referred to as Matsubara frequency modes), and the momentum integral in the dimensional regularization is cast into the form

$$\mu^\epsilon \int \frac{d^D k}{(2\pi)^D} \rightarrow \mu^\epsilon i T \sum_{n=-\infty}^{\infty} \int \frac{d^{D-1} k}{(2\pi)^{D-1}} \equiv \int_k \quad (2)$$

where $D = 4 - \epsilon$, μ is an arbitrary scale with a mass dimension one, $\omega_n = 2\pi n$ for bosons and $\omega_n = (2n + 1)\pi n$ for fermions with n being integers. Note that bosons have $\omega_0 = 0$ mode, which causes an infrared (IR) divergence problem as demonstrated in Section 3.

As is the case at zero temperature [111], the one-loop effective potential can be derived by

$$\mu^\epsilon V_1(\varphi; T) = \frac{1}{2} \int_K \ln(K^2 + \bar{m}^2) = \frac{1}{2} \int_k \ln(k^2 - \bar{m}^2) + \frac{T^4}{2\pi^2} I_{B,F}(a^2), \quad (3)$$

where φ is the classical field, \bar{m} is the φ -dependent mass, $K^2 = \omega_n^2 + \mathbf{k}^2$, the first term corresponds to the zero temperature effective potential, $\int_k = \mu^\epsilon \int \frac{d^D k}{(2\pi)^D}$ with $k^2 = (k^0)^2 - \mathbf{k}^2$, while the second term is finite temperature contribution and $I_{B,F}(a^2)$ are defined as

$$I_{B,F}(a^2) = \int_0^\infty dx x^2 \exp \left[1 \mp e^{-\sqrt{x^2+a^2}} \right], \quad (4)$$

with $a^2 = \bar{m}^2/T^2$. The high temperature expansions (HTE) of $I_{B,F}$ are, respectively, given by

$$I_B^{\text{HTE}}(a^2) = -\frac{\pi^4}{45} + \frac{\pi^2}{12} a^2 - \frac{\pi}{6} (a^2)^{3/2} - \frac{a^4}{32} \left(\log \frac{a^2}{\alpha_B} - \frac{3}{2} \right) + \mathcal{O}(a^6), \quad (5)$$

$$I_F^{\text{HTE}}(a^2) = \frac{7\pi^4}{360} - \frac{\pi^2}{24} a^2 - \frac{a^4}{32} \left(\log \frac{a^2}{\alpha_F} - \frac{3}{2} \right) + \mathcal{O}(a^6), \quad (6)$$

where $\ln \alpha_B = 2 \ln 4\pi - 2\gamma_E = 3.91$ and $\ln \alpha_F = 2 \ln \pi - 2\gamma_E = 1.14$. The general expressions of higher-order terms can be found in Ref. [11]. Numerical analysis shows that $|I_B(a^2) - I_B^{\text{HTE}}(a^2)| \lesssim 0.05$ if $a \lesssim 2.3$ and $|I_F(a^2) - I_F^{\text{HTE}}(a^2)| \lesssim 0.05$ for $a \lesssim 1.7$. With this expansions, one can see that $V_1(\varphi, T)$ includes $+c^2 \varphi^2 T^2$ with c being some coupling, which makes spontaneous broken symmetry restored at high temperature. In other words, the phase transition could exist at high temperature. If this is the case, the order of the phase transition is of our interest.

In Figure 1, first- and second-order phase transitions are depicted in upper and lower panels, respectively. In the left panels, the effective potentials are plotted as functions of φ while the temperature evolutions of the scalar VEV are shown in the right panels. In the first-order phase transition case, there exists discontinuity in the evolution of the vacuum and the critical temperature (T_C) is defined at a temperature at which V_{eff} has the degenerate minima separated by the potential barrier as shown in the upper left panel. v_C is the VEV at T_C , where T approaches T_C from below. What is important here is that the bosonic thermal loop contribution has the cubic term with a negative sign, $-(a^2)^{3/2} T^4 \simeq -|\varphi|^3 T$ (Here we assume that $\bar{m}^2 \propto \varphi^2$ such as gauge bosons or scalars in classical scale-invariant theories. In general, however, \bar{m}^2 can have an extra mass parameter, for instance in the ϕ^4 theory, $\bar{m}^2 = -m^2 + \lambda \varphi^2/2$, which will be discussed below) originated from the zero Matsubara frequency mode $\omega_0 = 0$, which can induce the potential barrier. In the second-order phase transition case, on the other hand, the temperature evolution of VEV is continuous but its first derivative with respect to the temperature has the singular behavior at T_C which is defined by the temperature at which the curvature at the origin becomes zero. Unlike the first-order phase transition, there is no potential barrier.

In gauge theories, V_{eff} is inherently gauge dependent. Nevertheless, it is shown that $\mathcal{O}(\varphi^2 T^2)$ term as well as energies at stationery points are gauge-fixing parameter independent. We discuss the gauge dependence issue in detail in Section 4.3.

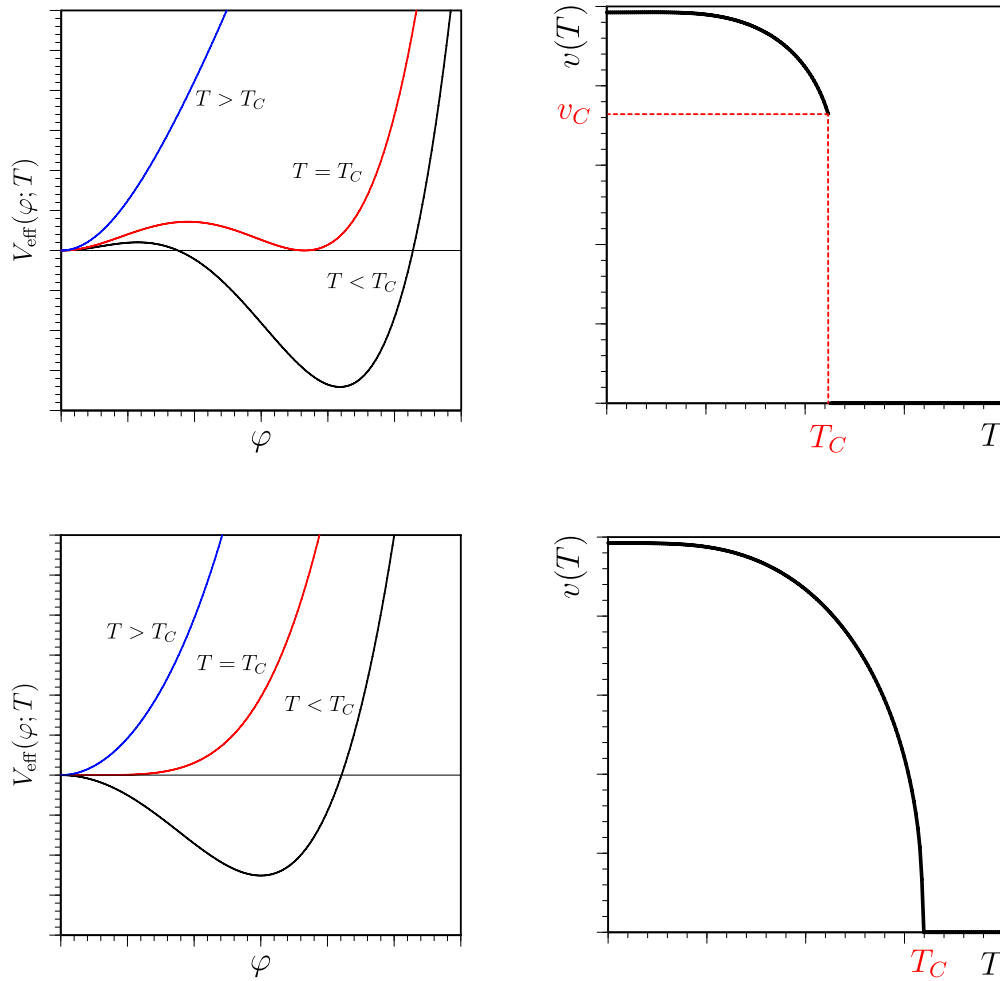


Figure 1. Two types of phase transitions. (Upper) Case of the first-order phase transition; shapes of the effective potential at $T > T_C$, $T = T_C$ and $T < T_C$ [left panel] and the temperature evolution of the VEV of scalar [right panel]. (Lower) Counterparts in the case of the second-order phase transition.

Before we discuss EWPT, we consider the ϕ^4 theory in order to see the symmetry behavior at high- T . The Lagrangian is given by

$$\mathcal{L} = \frac{1}{2} \partial_\mu \phi \partial^\mu \phi - V_0(\phi), \quad V_0(\phi) = -\frac{m^2}{2} \phi^2 + \frac{\lambda}{4!} \phi^4, \quad (7)$$

where $\lambda > 0$ and $m^2 > 0$. This model has the Z_2 symmetry, $\phi \rightarrow -\phi$, but it is spontaneously broken because of the $-m^2$ term. The field-dependent scalar mass is derived by $\bar{m}^2 = \partial^2 V_0 / \partial \phi^2 = -m^2 + \lambda \phi^2 / 2$. The one-loop effective potential in the $\overline{\text{MS}}$ scheme takes the form

$$V_1(\phi; T) = \frac{\bar{m}^4}{64\pi^2} \left(\ln \frac{\bar{m}^2}{\bar{\mu}^2} - \frac{3}{2} \right) + \frac{T^4}{2\pi^2} I_B(a^2), \quad (8)$$

where $\bar{\mu}^2 = 4\pi e^{-\gamma_E} \mu^2$ with γ_E being the Euler constant. Combining this with $V_0(\phi)$, one finds

$$V_{\text{eff}}(\phi; T) = V_0(\phi) + V_1(\phi; T) \\ \simeq -\frac{\pi^2 T^4}{90} + \frac{1}{2} \left(-m^2 + \frac{\lambda}{24} T^2 \right) \phi^2 - \frac{T}{12\pi} (\bar{m}^2)^{3/2} + \frac{\lambda}{4!} \phi^4 + \frac{\bar{m}^4}{64\pi^2} \left(\ln \frac{T^2}{\bar{\mu}^2} + 2c_B \right), \quad (9)$$

where $c_B = \ln \alpha_B / 2$ and HTE is used in the second line. One can find that the Z_2 symmetry can be restored at high temperature due to the positive contribution of the $\mathcal{O}(T^2)$ term. Presence of the $(\bar{m}^2)^{3/2}$

term may signify that the phase transition could be first order with the critical temperature of $T_C \simeq v_C/\sqrt{\lambda}$ if $(\bar{m}^2)^{3/2} \simeq \lambda^{3/2}\varphi^3$. Or, if the $(\bar{m}^2)^{3/2}$ term can be neglected, the phase transition would be reduced to the second order with the critical temperature of $T_C \simeq \sqrt{m^2/\lambda}$. As shown in the next section, the perturbative expansion would break down at around T_C even if $\lambda \ll 1$. Therefore, we cannot make any conclusion about the order of the phase transition from the above potential (9). We explicitly demonstrate why the perturbative expansion is invalidated at high temperature in the next section.

Before closing this section, we address an issue of the imaginary part of the effective potential. At $T = 0$, $\ln \bar{m}^2$ would give the imaginary part if $\bar{m}^2 < 0$. Its sign is determined by an $i\epsilon$ prescription for the propagator. Namely, $\ln(\bar{m}^2 - i\epsilon) = \ln\{|\bar{m}^2|(-1 - i\epsilon)\} = \ln|\bar{m}^2|e^{-i\pi} = \ln|\bar{m}^2| - i\pi$, and therefore the imaginary part of $V_1(\varphi; T = 0)$ in Equation (8) is [112]

$$\text{Im}V_1(\varphi; T = 0) = -\frac{\bar{m}^4}{64\pi}. \tag{10}$$

In the work of E. Weinberg and A. Wu [113], the imaginary part is interpreted as a decay rate of a state. Another interpretation is given by analogy with a Schwinger effect in Ref. [114]. Note that this imaginary part would be cancelled by a counterpart arising from the thermal function of I_B at high temperature, as indicated by Equation (9). Nevertheless, the effective potential (9) still can be complex since the $(\bar{m}^2)^{3/2}$ term gives another imaginary part if $\bar{m}^2 < 0$, which could be viewed as a harbinger of the breakdown of the perturbation theory. As discussed in the next section, the term would be modified as a consequence of the thermal resummation and the imaginary part could disappear at high temperature (see Equation (25) or Equation (28)).

3. Breakdown of Perturbative Expansion and Thermal Resummation

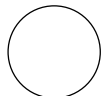
Let us consider some loop diagrams at high temperature. For illustrative purpose, we focus on the ϕ^4 theory [3] (for further developments that are not covered here, see, e.g., Ref. [46,115]). As is the $T = 0$ case, the mass term receives higher-order corrections as

$$\bar{M}^2 = \bar{m}^2 + \Sigma_\varphi(\varphi; T), \tag{11}$$

where $\Sigma_\varphi(\varphi; T)$ is the temperature-dependent self-energy. At one-loop order, one has

$$\bar{M}^2 = \bar{m}^2 + \frac{\lambda}{2}I(\bar{m}^2), \tag{12}$$

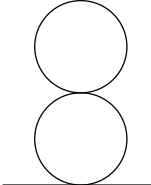
where



$$= \frac{\lambda}{2}I(\bar{m}^2) = \frac{\lambda}{2} \int_K \frac{1}{K^2 + \bar{m}^2} \xrightarrow{T>0} \frac{\lambda}{2} \frac{I'_B(a^2)}{\pi^2} = \frac{\lambda}{2} \left[\frac{T^2}{12} - \frac{T\bar{m}}{4\pi} + \dots \right], \tag{13}$$

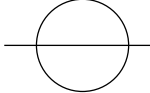
where $I'_B(a^2) = \partial I_B(a^2)/\partial a^2$ and $\bar{m} = (\bar{m}^2)^{1/2}$. Therefore, this diagram grows with $\mathcal{O}(T^2)$ at high temperature. The second term comes from the $\omega_0 = 0$ mode, which brings about the IR divergence discussed below. Now we estimate multi-loop diagrams by fully exploiting Equation (13). For the moment, we ignore the numerical coefficients to make our discussion simpler.

There exist two types of the 2-loop diagrams: the figure-8 and sunset diagrams. The figure-8 diagram is composed of one 1-vertex bubble (VB) and one 2VB. The former goes like λT^2 as seen from Equation (13) while the latter is estimated as $\lambda \int_K 1/(K^2 + \bar{m}^2)^2 = -\lambda \partial I(\bar{m}^2)/\partial \bar{m}^2 \sim \lambda T/\bar{m}$, which amounts to



$$\text{(figure-8)} \sim \lambda T^2 \left(\frac{\lambda T}{\bar{m}} \right). \quad (14)$$

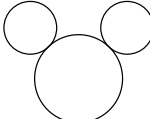
On the other hand, the sunset diagram in the high- T limit is roughly given by [116].



$$\text{(sunset)} \sim \lambda^2 T^2 \ln \frac{\bar{m}}{T}. \quad (15)$$

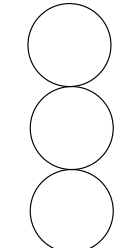
Comparing those two 2-loop diagrams, one finds that the figure-8 diagram becomes dominant at high temperature. Despite this fact, the sunset diagram plays an important role in studying the phase transition [116].

Attaching one more 1VB to the lower bubble in the figure-8 diagram, one gets a *mouse* diagram in which 3VB comes in. This new contribution is evaluated as $\lambda \int_{\mathcal{K}} 1/(K^2 + \bar{m}^2)^3 = (\lambda/2) \partial^2 I(\bar{m}^2)/\partial(\bar{m}^2)^2 \sim \lambda T/\bar{m}^3$. Thus we have



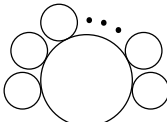
$$\text{(mouse)} \sim (\lambda T^2)^2 \left(\frac{\lambda T}{\bar{m}^3} \right). \quad (16)$$

On the other hand, if we attach one 1 VB to the upper bubble in the figure-8 diagram, it becomes a *cactus* diagram, which is composed of one 1 VB and two 2 VB. From the above estimates, it follows that



$$\text{(cactus)} \sim \lambda T^2 \left(\frac{\lambda T}{\bar{m}} \right)^2, \quad (17)$$

Taking the ratio of those two 3-loop diagrams, one finds that $\text{(mouse)}/\text{(cactus)} = T/\bar{m}$. Therefore, the mouse diagram becomes dominant at high temperature. We could have another 3-loop diagram which is made by attaching one 1 VB to the sunset diagram. However such a diagram cannot compete with the mouse diagram. Noting that whenever one 1 VB is attached to the lower bubble in the figure-8 diagram, one gets the factor of $\lambda T^2/\bar{m}^2$. Thus, a diagram that is composed of $(n - 1)$ 1 VB and one n VB (referred to as *daisy* diagram) is found to be



$$\text{(daisy)} \sim \frac{\lambda^2 T^3}{\bar{m}} \left(\frac{\lambda T^2}{\bar{m}^2} \right)^{n-2}. \quad (18)$$

Therefore, in addition to $\lambda < 1$, it needs $\lambda T^2/\bar{m}^2 < 1$ in order that the perturbative expansion makes sense. However, as discussed in Section 2, one has $T_C \simeq \bar{m}/\sqrt{\lambda}$ when the symmetry is restored, which means that the one-loop order calculation is not reliable in studying the phase transition. This demonstration suggests that one has to incorporate all the relevant diagrams into our calculation, that is, necessity of the resummation.

Let us redo the above analysis taking the numerical factor with care. The daisy diagram is actually given by

$$-i(\text{daisy}) = \left(\frac{-i\lambda}{2}\right)^n \left(\frac{T^2}{12}\right)^{n-1} \frac{(i\partial_{\bar{m}^2})^{n-1} I(\bar{m}^2)}{(n-1)!}, \quad (19)$$

where $\partial_{\bar{m}^2} = \partial/\partial(\bar{m}^2)$. Note that $n = 1$ is reduced to 1VB given in Equation (13). Summing up all the dominant diagrams at high temperature, the self-energy is calculated as

$$\begin{aligned} -i\Sigma_\varphi(\varphi; T) &= \sum_{n=1}^{\infty} \left(\frac{-i\lambda}{2}\right)^n \left(\frac{T^2}{12}\right)^{n-1} \frac{(i\partial_{\bar{m}^2})^{n-1} I(\bar{m}^2)}{(n-1)!} \\ &= \sum_{n=0}^{\infty} \left(\frac{-i\lambda}{2}\right)^{n+1} \left(\frac{T^2}{12}\right)^n \frac{(i\partial_{\bar{m}^2})^n I(\bar{m}^2)}{(n)!} \\ &= \left(\frac{-i\lambda}{2}\right) \exp\left(\frac{\lambda T^2}{24} \partial_{\bar{m}^2}\right) I(\bar{m}^2) = \left(\frac{-i\lambda}{2}\right) I\left(\bar{m}^2 + \frac{\lambda T^2}{24}\right) \\ &\simeq \frac{-i\lambda}{2} \left[\frac{T^2}{12} - \frac{T}{4\pi} \left(\bar{m}^2 + \frac{\lambda T^2}{24}\right)^{1/2} + \dots \right]. \end{aligned} \quad (20)$$

Therefore, the daisy resummation to leading order amounts to

$$\bar{M}^2 = \bar{m}^2 + \frac{\lambda}{2} I\left(\bar{m}^2 + \frac{\lambda T^2}{24}\right). \quad (21)$$

Including super-daisy diagrams [3,117], once arrives at a gap equation

$$\bar{M}^2 = \bar{m}^2 + \frac{\lambda}{2} I(\bar{M}^2). \quad (22)$$

Note that the sunset-type diagrams such as (15) are not included in the daisy and super-daisy resummations. In the study of the phase transition, however, such diagram cannot be neglected.

It should be emphasized that the resummation is merely re-organization of the perturbative expansion so that original Lagrangian is not changed at all. This can be seen as follows. Following the work of Parwani [118], let us decompose the bare Lagrangian (\mathcal{L}_B) into the renormalized one (\mathcal{L}_R) and corresponding counterterms (\mathcal{L}_{CT}) and then add and subtract the thermal mass correction of $\Sigma_\varphi(T)$ as

$$\mathcal{L}_B = \left[\mathcal{L}_R - \frac{1}{2} \Sigma_\varphi \varphi^2 \right] + \left[\mathcal{L}_{CT} + \frac{1}{2} \Sigma_\varphi \varphi^2 \right]. \quad (23)$$

We regard Σ_φ appearing in the renormalized Lagrangian as un-perturbed part while the latter as the part of the counterterm. In this *resummed Lagrangian*, the scalar propagator is given by $1/(K^2 + \bar{M}^2)$ with $\bar{M}^2 = \bar{m}^2 + \Sigma_\varphi$. Thus, the one-loop effective potential can be obtained by replacing \bar{m}^2 with \bar{M}^2 in Equation (8):

$$\mu^\epsilon V_{1+\text{daisy}}(\varphi; T) = \frac{1}{2} \int \frac{d^4k}{(2\pi)^4} \ln(K^2 + \bar{M}^2) = \frac{\bar{M}^4}{64\pi^2} \left(\ln \frac{\bar{M}^2}{\bar{\mu}^2} - \frac{3}{2} \right) + \frac{T^4}{2\pi^2} I_B \left(\frac{\bar{M}^2}{T^2} \right). \quad (24)$$

Putting all together and taking HTE, the effective potential in the Parwani scheme is reduced to

$$V_{\text{eff, Parwani}}^{\text{HTE}}(\varphi; T) = (\text{const}) - \frac{m^2}{2} \varphi^2 + \frac{\bar{m}^2}{24} T^2 - \frac{T}{12\pi} (\bar{M}^2)^{3/2} + \frac{\lambda}{4!} \varphi^4 + \frac{\bar{M}^4}{64\pi^2} \left(\ln \frac{T^2}{\bar{\mu}^2} + 2c_B \right), \quad (25)$$

where (const) denotes the φ -independent terms that are irrelevant to the phase transition.

Recalling that the IR divergence is originated from the $\omega_0 = 0$ mode, we could resum only this mode (Arnold-Espinosa (AE) scheme) [116]. In this scheme, the resummed effective potential is cast into the form

$$\begin{aligned}
\mu^\epsilon V_{1+\text{daisy}} &= \frac{1}{2} \sum' \ln(K^2 + \bar{m}^2) + \frac{T}{2} \int \frac{d^{D-1}\mathbf{k}}{(2\pi)^{D-1}} \ln(\mathbf{k}^2 + \bar{M}^2) \\
&= \frac{1}{2} \sum' \ln(K^2 + \bar{m}^2) + \frac{T}{2} \int \frac{d^{D-1}\mathbf{k}}{(2\pi)^{D-1}} \left[\ln(\mathbf{k}^2 + \bar{M}^2) - \ln(\mathbf{k}^2 + \bar{m}^2) \right] \\
&= \mu^\epsilon V_1(\varphi; T) + V_{\text{daisy}}(\varphi; T),
\end{aligned} \tag{26}$$

where \sum' in the first line is the summation over n without $\omega_0 = 0$ mode, the first term in the second line is the same as the unresummed one-loop effective potential given in Equation (8) while the second term is the daisy resummation, which reads

$$V_{\text{daisy}}(\varphi; T) = -\frac{T}{12\pi} \left[(\bar{M}^2)^{3/2} - (\bar{m}^2)^{3/2} \right]. \tag{27}$$

In the AE scheme, the total effective potential using HTE is cast into the form

$$V_{\text{eff, AE}}^{\text{HTE}}(\varphi; T) = (\text{const}) - \frac{m^2}{2} \varphi^2 + \frac{\bar{m}^2}{24} T^2 - \frac{T}{12\pi} (\bar{M}^2)^{3/2} + \frac{\lambda}{4!} \varphi^4 + \frac{\bar{m}^4}{64\pi^2} \left(\ln \frac{T^2}{\bar{\mu}^2} + 2c_B \right), \tag{28}$$

where (const) denotes the φ -independent terms. This resummed potential agrees with that in the Parwani scheme Equation (25) except for the last term. Comparisons between the two resummation schemes in a model of the SM extension can be found in Ref. [75] (for a recent study, see, e.g., Ref. [119]).

Here, we make a comment on the order of the phase transition in the ϕ^4 theory. It is known from the general argument of renormalization group analysis that the phase transition is second order [120]. In contrast to this, perturbative calculations could give a different answer. For instance, if one uses the effective potential with the daisy resummation shown here or super-daisy resummation, the phase transition is first order [117,121,122]. Beyond those resummations including the sunset-type diagrams, however, it turns into the second-order phase transition [123–125], which is consistent with the aforementioned general argument.

Before closing this section, we briefly discuss the resummation in gauge theories. At finite temperature, the Lorentz symmetry is broken by thermal bath specified by a four vector of u^μ , which takes the form of $u^\mu = (1, \mathbf{0})$ in the rest frame of thermal bath. Consequently, the gauge boson polarization tensor $\Pi_{\mu\nu}(p^0, \mathbf{p})$ is constructed by four basis tensors $\{g_{\mu\nu}, p_\mu p_\nu, u_\mu u_\nu, p_\mu u_\nu + p_\nu u_\mu\}$. It is convenient to define $u_\mu^T = u_\mu - (p \cdot u) p_\mu / p^2$ such that $u_\mu^T p^\mu = 0$. With those four basis tensors, $\Pi_{\mu\nu}(p^0, \mathbf{p})$ is generally written as

$$\Pi_{\mu\nu}(p^0, \mathbf{p}) = \Pi_L(p^0, \mathbf{p}) L_{\mu\nu}(p) + \Pi_T(p^0, \mathbf{p}) T_{\mu\nu}(p) + \Pi_G(p^0, \mathbf{p}) G_{\mu\nu}(p) + \Pi_S(p^0, \mathbf{p}) S_{\mu\nu}(p), \tag{29}$$

where

$$L_{\mu\nu}(p) = \frac{u_\mu^T u_\nu^T}{(u^T)^2}, \quad T_{\mu\nu}(p) = g_{\mu\nu} - \frac{p_\mu p_\nu}{p^2} - L_{\mu\nu}(p), \tag{30}$$

$$G_{\mu\nu}(p) = \frac{p_\mu p_\nu}{p^2}, \quad S_{\mu\nu}(p) = \frac{p_\mu u_\nu^T + p_\nu u_\mu^T}{\sqrt{(p \cdot u)^2 - p^2}}. \tag{31}$$

Note that both $L_{\mu\nu}$ and $T_{\mu\nu}$ are 4-dimensionally transverse while the former (the latter) are 3-dimensionally longitudinal (transverse). In Landau gauge ($\xi = 0$), the resummed gauge boson propagator has the form

$$D_{\mu\nu}(p) = \frac{-L_{\mu\nu}(p)}{p^2 - m^2 - \Pi_L(p^0, \mathbf{p})} + \frac{-T_{\mu\nu}(p)}{p^2 - m^2 - \Pi_T(p^0, \mathbf{p})}, \tag{32}$$

where m is the gauge boson mass at $T = 0$. Here, two kind of the gauge boson thermal masses are defined as

$$\Delta m_L^2 = \lim_{p \rightarrow 0} \lim_{p^0 \rightarrow 0} \Pi_L(p^0, \mathbf{p}), \quad \Delta m_T^2 = \lim_{p \rightarrow 0} \lim_{p^0 \rightarrow 0} \Pi_T(p^0, \mathbf{p}). \quad (33)$$

The former is called *electric mass* and the latter *magnetic mass*. It should be noted that the order of taking limits is not exchangeable. The opposite limit give different results [126]. As well known, the electric mass can arise perturbatively, which is the order of gT with g being a gauge coupling. However, it is proven that the magnetic mass does not arise in abelian gauge theories to all orders [126]. In non-abelian gauge theories, on the other hand, the magnetic mass can be generated though its evaluation requires non-perturbative methods [127]. Unlike the electric mass, the order of the magnetic mass is g^2T .

Thermal resummation in non-abelian gauge theories is formulated as Hard Thermal Loop (HTL) perturbation theory [128–131], which can resum leading $\mathcal{O}(T^2)$ corrections in a gauge-invariant way. This method has been applied to quantum chromodynamics (QCD). In EW theories, on the other hand, there exist additional mass scales coming from the Higgs and/or new particles beyond the SM, and thus the presumed scale hierarchy in HTL does not always hold. In this article, we do not cover details of HTL and other related topics, and readers are referred to Refs. [126,127,132–136].

4. Electroweak Phase Transition

The discovery of the Higgs boson in 2012 has completed the particle content of the SM, and its mass measurement is the first step towards the re-construction of the Higgs potential. In order to confirm the role of the Higgs boson as the EW symmetry breaker, the measurement of the Higgs self-coupling is indispensable. For the detectability at future high-energy colliders, see, e.g., Refs. [137–139]. As discussed in the previous section, the symmetry can be restored at high temperature, implying that EWPT can occur at early epoch of the Universe. If this is the case, a question of our interest is how it takes place, i.e., *what is the order of EWPT?* In this section, we discuss a case of first-order EWPT, which is a dramatic event for cosmology. We exemplify a case in which intermediate breaking of a Z_2 symmetry at finite temperature plays a pivotal role in realizing the first-order EWPT.

4.1. Standard Model

We start by discussing EWPT in the SM. Tree-level Higgs potential is comprised of the following two gauge-invariant terms:

$$V_0(H) = -\mu_H^2 H^\dagger H + \lambda_H (H^\dagger H)^2, \quad (34)$$

where $\mu_H^2 >$ and $\lambda_H > 0$ are presumed. We denote the Higgs doublet field with a hypercharge 1/2 as

$$H(x) = \left(\begin{array}{c} G^+(x) \\ \frac{1}{\sqrt{2}}(v + h(x) + iG^0(x)) \end{array} \right), \quad (35)$$

where $v = 246$ GeV, h denotes the Higgs boson with a mass of 125 GeV, and $G^{0,\pm}$ are the Nambu-Goldstone (NG) bosons that are absorbed into the longitudinal components of the Z and W^\pm bosons. The vacuum is determined by the stationary condition of

$$\left\langle \frac{\partial V_0}{\partial h} \right\rangle = v \left[-\mu_H^2 + \lambda_H v^2 \right] = 0, \quad (36)$$

where $\langle X \rangle$ denotes X is evaluated in the vacuum where the fluctuation fields are zero, enforcing $\mu_H^2 = \lambda_H v^2$. In the vacuum, the Higgs boson mass is given by

$$m_h^2 = \left\langle \frac{\partial^2 V_0}{\partial h^2} \right\rangle = -\mu_H^2 + 3\lambda_H v^2 = 2\lambda_H v^2 \quad (37)$$

where the vacuum condition is used to eliminate μ_H^2 .

Let us denote the classical constant background field as φ . From Equation (34), the tree-level effective potential is given by

$$V_0(\varphi) = -\frac{\mu_H^2}{2}\varphi^2 + \frac{\lambda_H}{4}\varphi^4. \quad (38)$$

As is the calculation in the ϕ^4 theory, the one-loop effective potential without thermal resummation is written as

$$V_1(\varphi; T) = V_{\text{CW}}(\varphi) + \sum_i n_i \frac{T^4}{2\pi^2} I_{B,F} \left(\frac{\bar{m}_i^2}{T^2} \right), \quad (39)$$

with

$$V_{\text{CW}}(\varphi) = \sum_i n_i \frac{\bar{m}_i^4}{64\pi^2} \left(\ln \frac{\bar{m}_i^2}{\bar{\mu}^2} - c_i \right) \quad (40)$$

where $i = h, G^0, G^\pm, W, Z, t$, $V_{\text{CW}}(\varphi)$ is regularized by the $\overline{\text{MS}}$ scheme, n_i are the degrees of freedom with a statistics: $n_h = n_{G^0} = 1$, $n_{G^\pm} = 2$, $n_W = 6$, $n_Z = 3$ and $n_t = -12$. $c_i = 3/2$ for scalars and fermions while $c_i = 5/6$ for gauge bosons. The explicit forms of the field-dependent masses are

$$\bar{m}_h^2 = -\mu_H^2 + 3\lambda_H\varphi^2, \quad \bar{m}_{G^0}^2 = \bar{m}_{G^\pm}^2 = -\mu_H^2 + \lambda_H\varphi^2, \quad (41)$$

$$\bar{m}_W^2 = \frac{g_2^2}{4}\varphi^2, \quad \bar{m}_Z^2 = \frac{g_2^2 + g_1^2}{4}\varphi^2, \quad \bar{m}_t^2 = \frac{y_t^2}{2}\varphi^2, \quad (42)$$

where g_2, g_1 and y_t are the $SU(2)_L, U(1)_Y$ and top Yukawa couplings, respectively. The masses in the vacuum are obtained by $m_i^2 = \langle \bar{m}_i^2 \rangle = \bar{m}_i^2|_{\varphi=v}$.

The vacuum and Higgs boson mass at one-loop level in the $\overline{\text{MS}}$ scheme are defined by the conditions:

$$0 = \left\langle \frac{\partial(V_0 + V_{\text{CW}})}{\partial\varphi} \right\rangle = (-\mu_H^2 + \lambda_H v^2)v + \left\langle \frac{\partial V_{\text{CW}}}{\partial\varphi} \right\rangle, \quad (43)$$

$$m_h^2 = \left\langle \frac{\partial^2(V_0 + V_{\text{CW}})}{\partial\varphi^2} \right\rangle = 2\lambda_H v^2 + \left\langle \frac{\partial^2 V_{\text{CW}}}{\partial\varphi^2} \right\rangle - \frac{1}{v} \left\langle \frac{\partial V_{\text{CW}}}{\partial\varphi} \right\rangle. \quad (44)$$

Note that the relationship between the $\overline{\text{MS}}$ Higgs boson mass and the on-shell (OS) mass (M_h) is given by

$$M_h^2 = m_h^2 + \Delta\Sigma_h(M_h), \quad (45)$$

where $\Delta\Sigma_h(M_h) = \text{Re}\bar{\Sigma}_h(M_h) - \text{Re}\bar{\Sigma}_h(0)$ with $\bar{\Sigma}_h$ being the self-energy of the Higgs boson regularized by the $\overline{\text{MS}}$ scheme. Note that all the parameters except M_h in Equation (45) are the $\overline{\text{MS}}$ running parameters that are governed by renormalization group equations. One can show that M_h^2 is independent of $\bar{\mu}$ by noting that

$$\frac{dm_h^2}{d\ln\bar{\mu}} = 2\gamma_h m_h^2, \quad \frac{d\Delta\Sigma_h(M_h)}{d\ln\bar{\mu}} = -2\gamma_h m_h^2, \quad (46)$$

where γ_h is the anomalous dimension of the Higgs field. At one-loop order, we actually have

$$\frac{dm_{h,1\text{-loop}}^2}{d\ln\bar{\mu}} \simeq 2\gamma_h^{(1)} m_{h,\text{tree}}^2, \quad \frac{d\Delta^{(1)}\Sigma_h(M_h)}{d\ln\bar{\mu}} \simeq -2\gamma_h^{(1)} m_{h,\text{tree}}^2 \quad (47)$$

where $m_{h,1\text{-loop}}^2$ is given by Equation (44), $m_{h,\text{tree}}^2 = 2\lambda_H v^2$ and $\gamma_h^{(1)} \simeq [-3(3g_2^2 + g_1^2)/4 + 3y_t^2]/(16\pi^2)$. From those, it follows that $dM_h^2/d\ln\bar{\mu} = 0$ at one-loop level.

We note in passing that in the SM, the one-loop correction of $\Delta\Sigma_h(M_h)$ is rather minor if $\bar{\mu}$ is evaluated at the pole mass of the top quark.

Another renormalization conditions often used in the literature is ‘‘OS-like’’ renormalization in which [5,75]

$$\left\langle \frac{\partial(V_{\text{CW}} + V_{\text{CT}})}{\partial\varphi} \right\rangle = 0, \quad \left\langle \frac{\partial^2(V_{\text{CW}} + V_{\text{CT}})}{\partial\varphi^2} \right\rangle = 0, \tag{48}$$

where $V_{\text{CT}} = -\delta\mu_H^2\varphi^2/2$. Those two conditions determine $\delta\mu_H^2$ and $\bar{\mu}$ as

$$\delta\mu^2 = \frac{1}{v} \left\langle \frac{\partial V_1}{\partial\varphi} \right\rangle, \quad \bar{\mu} = \exp \left[\frac{\sum_i \langle \bar{m}_i^{\prime 2} \rangle^2 (\ln m_i^2 - c_i + 3/2)}{2 \sum_i \langle \bar{m}_i^{\prime 2} \rangle^2} \right], \tag{49}$$

where $\langle \bar{m}_i^{\prime 2} \rangle - \langle \bar{m}_i^{\prime 2} \rangle/v = 0$ is used in $\bar{\mu}$. With those, the effective potential at one-loop level takes the form

$$V_{\text{CW}}(\varphi) = \sum_i \frac{n_i}{64\pi^2} \left[2m_i^2 \bar{m}_i^2 + \bar{m}_i^4 \left(\ln \frac{\bar{m}_i^2}{m_i^2} - \frac{3}{2} \right) \right]. \tag{50}$$

Note that this scheme is not exactly the same as the OS scheme since the mass is not defined at the pole position of the Higgs boson propagator as given above. By ‘‘OS-like’’, we mean that tree-level relations among the model parameters such as $m_h^2 = 2\lambda_H v^2$ hold even at higher orders as is the genuine OS renormalization. We quantify numerical impacts of the scheme dependences on EWPT in Section 4.4. In what follows, we employ the OS-like scheme.

Aside from numerical accuracy, HTEs of $I_{B,F}$ make it easy to discuss physics. The high- T expanded effective potential is cast into the form

$$V_{\text{eff}}(\varphi; T) = V_0(\varphi) + V_1(\varphi; T) \simeq D(T^2 - T_0^2)\varphi^2 - ET|\varphi|^3 + \frac{\lambda_T}{4}\varphi^4 + \dots, \tag{51}$$

where

$$T_0^2 = \frac{1}{D} \left(\frac{1}{4}m_h^2 - 2Bv^2 \right), \tag{52}$$

$$B = \frac{3}{64\pi^2 v^4} \left(2m_W^4 + m_Z^4 - 4m_t^4 \right), \tag{53}$$

$$D = \frac{1}{8v^2} \left(2m_W^2 + m_Z^2 + 2m_t^2 \right), \tag{54}$$

$$E = \frac{1}{4\pi v^3} \left(2m_W^3 + m_Z^3 \right), \tag{55}$$

$$\lambda_T = \frac{m_h^2}{2v^2} \left[1 - \frac{3}{8\pi^2 v^2 m_h^2} \left\{ 2m_W^4 \log \frac{m_W^2}{\alpha_B T^2} + m_Z^4 \log \frac{m_Z^2}{\alpha_B T^2} - 4m_t^4 \log \frac{m_t^2}{\alpha_F T^2} \right\} \right]. \tag{56}$$

Appearance of the cubic term signals that EWPT is first order. Its critical temperature T_C satisfies

$$V_{\text{eff}}(0; T_C) = V_{\text{eff}}(v_C; T_C), \quad \left. \frac{\partial V_{\text{eff}}(\varphi; T_C)}{\partial\varphi} \right|_{\varphi=0} = \left. \frac{\partial V_{\text{eff}}(\varphi; T_C)}{\partial\varphi} \right|_{\varphi=v_C}, \tag{57}$$

from which, one gets

$$T_C = \frac{T_0}{\sqrt{1 - E^2/(\lambda_{T_C} D)}}, \quad v_C = \frac{2ET_C}{\lambda_{T_C}}, \tag{58}$$

Note that $T_0 < T_C$ due to the presence of E . In the case of second-order EWPT in which $E = 0$, T_0 becomes the critical temperature. Straightforward numerical calculations show that $T_0 \simeq 163.1$ GeV, $B \simeq -4.4 \times 10^{-3}$, $D \simeq 0.17$, $E \simeq 9.6 \times 10^{-3}$ and $\lambda_{T_C} \simeq m_h^2 / (2v^2) \simeq 0.13$, which leads to $T_C \simeq 163.4$ GeV and $v_C \simeq 24.3$ GeV, where $m_h = 125.0$ GeV, $m_W = 80.4$ GeV, $m_Z = 91.2$ GeV and $m_t = 172.9$ GeV are used [6].

In the context of EWBG, to avoid the washout of the created BAU after EWPT, one has to have

$$\frac{v_C}{T_C} = \frac{2E}{\lambda_{T_C}} \gtrsim 1. \quad (59)$$

However, from the above numerical analysis one has $v_C/T_C \simeq 0.15$. Therefore, the EWBG possibility is excluded in the SM. We note in passing that if the Higgs boson is the free parameter and other particles masses are fixed to the observed values, one finds $m_h \lesssim 48$ GeV. To circumvent this difficulty, enhanced E and/or suppressed λ_{T_C} are necessary. This can be realized in the extension of the SM, as discussed in the next section.

Before moving to beyond the SM, we give some remarks on the above results.

- The above demonstration does not take the thermal resummation into consideration. If one performs it by either the Parwani or AE scheme, E would be diminished by the resummation effect as discussed in Section 3.
- The effective potential is the sum of 1-particle-irreducible diagrams by definition, which is inherently gauge dependent, and so the VEV defined by the minimum of the effective potential depends on a choice of specific gauge. This is natural consequence since the normalization of the scalar fields (wavefunction renormalization) is missing. Notwithstanding, energies at stationary points are gauge independent obeyed by the NFK identity [109,110].
- Since the phase transition is generically non-perturbative phenomenon, lattice calculations are more suitable to obtain robust results. It is shown in Refs. [140–143] that EWPT turns into smooth crossover for $m_h \gtrsim 73$ GeV. After the Higgs boson discovery, EWPT is re-analyzed in Ref. [144] in a different context. The “critical temperature” is found to be $T_C = 159.5 \pm 1.5$ GeV.

4.2. Standard Model with a Real Scalar

As discussed in the previous section, the parameter space of the strong first-order EWPT ($v_C/T_C \gtrsim 1$) in the SM is not consistent with the observed Higgs boson. One of the simplest extensions of the SM is to add a real scalar field that is singlet under the SM gauge group $SU(3)_C \times SU(2)_L \times U(1)_Y$ (referred to as rSM). As first emphasized by Funakubo et al. in the next-to-minimal supersymmetric SM [97], such a singlet scalar can increase the possibility of the first-order EWPT owing to multi-step transitions. In addition to this, the singlet scalar can be DM if the model is Z_2 symmetric. (The Z_2 symmetry is phenomenologically introduced to have the DM candidate. Since its origin is highly model dependent, we do not specify it in this review). Note that even though the Z_2 symmetry is preserved at $T = 0$, it does not necessarily hold at $T > 0$ depending on thermal history of the vacuum evolution. In what follows, we discuss two types of phase transitions as shown in Figure 2.

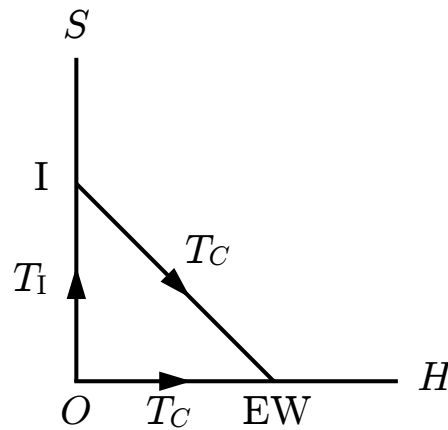


Figure 2. 2 patterns of the phase transitions in the presence of the SM Higgs and real scalar fields: (i) $O \rightarrow EW$ (1-step transition) and (ii) $O \rightarrow I \rightarrow EW$ (2-step transitions). In the latter case, the Z_2 symmetry is spontaneously broken in the intermediate phase (I phase) while restored in the EW phase, and S can become DM.

Let us denote the singlet scalar as S . The extended Higgs potential is cast into the form

$$V_0(H, S) = -\mu_H^2 H^\dagger H + \lambda_H (H^\dagger H)^2 - \frac{\mu_S^2}{2} S^2 + \frac{\lambda_S}{4} S^4 + \frac{\lambda_{HS}}{2} H^\dagger H S^2 \quad (60)$$

where H is given in Equation (35). The stationary conditions of H and S are, respectively, given by

$$\left\langle \frac{\partial V_0}{\partial h} \right\rangle = v \left[-\mu_H^2 + \lambda_H v^2 + \frac{\lambda_{HS}}{2} v_S^2 \right] = 0, \quad (61)$$

$$\left\langle \frac{\partial V_0}{\partial S} \right\rangle = v_S \left[-\mu_S^2 + \lambda_S v_S^2 + \frac{\lambda_{HS}}{2} v^2 \right] = 0. \quad (62)$$

where v_S is VEV of S . By assumption, the Z_2 symmetry is preserved at $T = 0$, which enforces $v_S = 0$. The Higgs boson masses at tree level take the form

$$m_h^2 = -\mu_H^2 + 3\lambda_H v^2 = 2\lambda_H v^2, \quad (63)$$

$$m_S^2 = -\mu_S^2 + \frac{\lambda_{HS}}{2} v^2. \quad (64)$$

Denoting the classical constant background fields of the doublet and singlet scalars as φ and φ_S , the effective potential at tree level is given by

$$V_0(\varphi, \varphi_S) = -\frac{\mu_H^2}{2} \varphi^2 + \frac{\lambda_H}{4} \varphi^4 + \frac{\lambda_{HS}}{4} \varphi^2 \varphi_S^2 - \frac{\mu_S^2}{2} \varphi_S^2 + \frac{\lambda_S}{4} \varphi_S^4. \quad (65)$$

To avoid the unbounded from below in the φ and φ_S directions, $\lambda_H > 0$ and $\lambda_S > 0$ are imposed. Moreover, the case of $\lambda_{HS} < 0$ needs additional condition. Denoting $\varphi_S = \delta\varphi$ with δ being a real parameter, the quartic terms in the Higgs potential can be written as

$$V_0(\varphi, \varphi_S) = \frac{1}{4} (\lambda_H + \lambda_{HS} \delta^2 + \lambda_S \delta^4) \varphi^4. \quad (66)$$

The coefficient of φ^4 has to be positive for any δ , which leads to $\lambda_{HS}^2 < 4\lambda_H \lambda_S$.

For $\mu_S^2 > 0$, a local minimum can appear in the singlet scalar direction, developing \bar{v}_S . For the EW vacuum to be the global minimum, one must have $V_0(v, 0) < V_0(0, \bar{v}_S)$, resulting in

$$\lambda_S > \lambda_H \frac{\mu_S^4}{\mu_H^4} = \frac{2}{m_H^2 v^2} \left(m_S^2 - \frac{\lambda_{HS}}{2} v^2 \right)^2 \equiv \lambda_S^{\min}. \quad (67)$$

In the rSM, only 3 free parameters exist. We consider m_S , λ_{HS} and λ_S as the input parameters in the following discussion.

First, we consider a simplified potential

$$V(\varphi, \varphi_S; T) = V_0(\varphi, \varphi_S) + \frac{1}{2} \Sigma_H(T) \varphi^2 + \frac{1}{2} \Sigma_S(T) \varphi_S^2 - ET\varphi^3, \quad (68)$$

where $\Sigma_H(T)$ and $\Sigma_S(T)$ are the thermal masses of H and S , which are, respectively, given by [32]

$$\Sigma_H(T) = \left[\frac{\lambda_H}{2} + \frac{\lambda_{HS}}{24} + \frac{3g_2^2 + g_1^2}{16} + \frac{y_t^2}{4} \right] T^2, \quad (69)$$

$$\Sigma_S(T) = \left[\frac{\lambda_S}{4} + \frac{\lambda_{HS}}{6} \right] T^2. \quad (70)$$

We begin with discussing a case in which the phase transition occurs only once (1-step transition scenario). It is convenient that the two scalar fields are parametrized in polar coordinates: $\varphi = z \cos \gamma$ and $\varphi_S = z \sin \gamma$, where $0 \leq \gamma \leq \pi/2$. Hereafter we use shorthand notations: $s_\gamma = \sin \gamma$ and $c_\gamma = \cos \gamma$. At T_C , one finds that $V(z, \gamma; T_C) = c_4 z^2 (z - z_C)^2$ with c_4 being $(\lambda_H c_{\gamma_C}^4 + \lambda_{HS} s_{\gamma_C}^2 c_{\gamma_C}^2 + \lambda_S s_{\gamma_C}^4)/4$, yielding

$$\frac{v_C}{T_C} = \frac{z_C}{T_C} c_{\gamma_C} = \frac{Ec_{\gamma_C}^4}{(\lambda_H c_{\gamma_C}^4 + \lambda_{HS} s_{\gamma_C}^2 c_{\gamma_C}^2 + \lambda_S s_{\gamma_C}^4)/2}. \quad (71)$$

Therefore, the strength of the first-order EWPT can be enhanced for $\lambda_{HS} < 0$.

Now we move on to discuss another case in which the phase transitions occur twice (2-step transition scenario). In this case, the phase transition prior to EWPT can be described by the potential

$$V_0(\varphi_S) = \frac{1}{2} (-\mu_S^2 + \Sigma_S(T)) \varphi_S^2 + \frac{\lambda_S}{4} \varphi_S^4. \quad (72)$$

The local minimum appears if $\mu_S^2 > \Sigma_S(T)$, which is given by $\tilde{v}_S^2 = (\mu_S^2 - \Sigma_S)/\lambda_S$. Note that the critical temperature in this case (denoted as T_I) is given by $\mu_S^2 = \Sigma_S(T_I)$, i.e.,

$$T_I^2 = \frac{\mu_S^2}{\lambda_S/4 + \lambda_{HS}/6}. \quad (73)$$

To analyze EWPT, we use the polar coordinates $\varphi = z c_\gamma$ and $\varphi_S = z s_\gamma + \tilde{v}_S$. Repeating the similar calculation as the case of the 1-step transition scenario, one can find

$$\frac{v_C}{T_C} = \frac{z_C}{T_C} c_{\gamma_C} = \frac{Ec_{\gamma_C}^4 - s_{\gamma_C} c_{\gamma_C} \tilde{v}_S [\lambda_{HS} c_{\gamma_C}^2/2 + \lambda_S s_{\gamma_C}^2]}{(\lambda_H c_{\gamma_C}^4 + \lambda_{HS} s_{\gamma_C}^2 c_{\gamma_C}^2 + \lambda_S s_{\gamma_C}^4)/2}. \quad (74)$$

Owing to SSB of the Z_2 symmetry, additional terms proportional to \tilde{v}_S appear in the numerator. Consequently, the first-order EWPT can be strengthened if $\lambda_{HS} > 0$ together with $s_{\gamma_C} < 0$, which is stark contrast to the 1-step transition scenario. Note that while \tilde{v}_S can get larger for smaller λ_S as shown above, the smallness of λ_S is limited by the global minimum condition (67).

Without the simplification, the one-loop effective potential in the $\overline{\text{MS}}$ scheme is given by

$$V_1(\varphi, \varphi_S; T) = \sum_i n_i \left[V_{\text{CW}}(\tilde{m}_i^2) + \frac{T^4}{2\pi^2} I_{B,F} \left(\frac{\tilde{m}_i^2}{T^2} \right) \right], \quad (75)$$

where $i = H_{1,2}, G^0, G^\pm, W, Z, t$. In the numerical study shown in Section 4.4, we adopt the Parwani scheme for the thermal resummation.

4.3. Perturbative Gauge-Invariant Treatment for the Thermal Phase Transitions

As briefly discussed in Section 4.1, the treatment of EWPT shown above suffers from the gauge dependence problem. Here, we introduce two gauge-invariant methods: high- T potential (HT) scheme and Patel-Ramsey-Musolf (PRM) scheme [145] and apply them to the 2-step transition scenario in the rSM.

Given the fact that the leading thermal mass is gauge independent, the simplest gauge-invariant effective potential is constructed by adding the thermal quadratic terms into the tree-level Higgs potential, which is nothing but the potential (68) without the cubic term:

$$V^{\text{HT}}(\varphi, \varphi_S; T) = V_0(\varphi, \varphi_S) + \frac{1}{2}\Sigma_H(T)\varphi^2 + \frac{1}{2}\Sigma_S(T)\varphi_S^2. \quad (76)$$

In this method, the 1-step scenario always induces the second-order EWPT while the 2-step transition scenario could accommodate the first-order EWPT depending on the parameter choices, as understood from the analysis in Section 4.2. In spite of the gauge-invariant construction, the main drawback here is lack of the quantum corrections that could be relevant. We quantify this statement in Section 4.4.

In contrast to this, the PRM scheme can take account of the quantum corrections to T_C based on the NFK identity. The statement of this identity is that energies at stationary points of the effective potential are gauge independent, i.e.,

$$\frac{\partial V_{\text{eff}}(\varphi, \xi)}{\partial \xi} = -C(\varphi, \xi) \frac{\partial V_{\text{eff}}(\varphi, \xi)}{\partial \varphi}, \quad (77)$$

where ξ is the gauge-fixing parameter and $C(\varphi, \xi)$ is some functional. While the statement is very simple, it needs some caution when we work in the perturbation theory. To derive the NFK identity at given order, we expand $V_{\text{eff}}(\varphi, \xi)$ and $C(\varphi, \xi)$ in powers of \hbar as

$$V_{\text{eff}}(\varphi, \xi) = V_0(\varphi) + \hbar V_1(\varphi, \xi) + \hbar^2 V_2(\varphi, \xi) + \dots, \quad (78)$$

$$C(\varphi, \xi) = c_0 + \hbar c_1(\varphi, \xi) + \hbar^2 c_2(\varphi, \xi) + \dots. \quad (79)$$

At tree level, there is no ξ dependence so that c_0 must vanish. At one-loop level, $\mathcal{O}(\hbar)$, on other hand, one can find

$$\frac{\partial V_1}{\partial \xi} = -c_1 \frac{\partial V_0}{\partial \varphi}. \quad (80)$$

It should be noted that the ξ dependence of V_1 vanishes at the stationary points of V_0 rather than V_1 . Let us look into the ξ dependence of V_1 more explicitly. The one-loop effective potential in the R_ξ gauge may contain the following ξ -dependent pieces:

$$V_1(\varphi; T) \ni \frac{(\bar{m}_G^2 + \xi \bar{m}_V^2)^2}{64\pi^2} \left(\ln \frac{\bar{m}_G^2 + \xi \bar{m}_V^2}{\bar{\mu}^2} - \frac{3}{2} \right) - \frac{(\xi \bar{m}_V^2)^2}{64\pi^2} \left(\ln \frac{\xi \bar{m}_V^2}{\bar{\mu}^2} - \frac{3}{2} \right) + \frac{T^4}{2\pi^2} \left[I_B \left(\frac{\bar{m}_G^2 + \xi \bar{m}_V^2}{T^2} \right) - I_B \left(\frac{\xi \bar{m}_V^2}{T^2} \right) \right], \quad (81)$$

where \bar{m}_V^2 and \bar{m}_G^2 are the field-dependent masses of the gauge and NG bosons. The ξ dependence would disappear at the point of $\bar{m}_G^2 = 0$, namely, $\langle \partial V_0 / \partial \varphi \rangle = 0$, satisfying the NFK identity at one-loop order. On the other hand, the vacuum condition used in the usual perturbative analysis,

for example in the $\overline{\text{MS}}$ scheme, is $\langle \partial(V_0 + V_1)/\partial\varphi \rangle = 0$ as given in Equation (43), which thus leads to the ξ -dependent result.

In the PRM scheme in the rSM, T_C at one-loop level is determined by the degeneracy condition

$$V_0(0, \tilde{v}_{S,\text{tree}}) + V_1(0, \tilde{v}_{S,\text{tree}}; T_C) = V_0(v_{\text{tree}}, v_{S,\text{tree}}) + V_1(v_{\text{tree}}, v_{S,\text{tree}}; T_C), \quad (82)$$

where $v_{\text{tree}} = 246$ GeV, $v_{S,\text{tree}} = 0$ and $\tilde{v}_{S,\text{tree}}$ is the minimum of $V_0(0, \varphi_S)$. Unlike the usual condition of T_C , the field values are fixed to their tree-level minima at $T = 0$. Since $V_{\text{eff}}(v_{1\text{-loop}}, v_{S,1\text{-loop}}; T) < V_{\text{eff}}(v_{\text{tree}}, v_{S,\text{tree}}; T)$, where $v_{1\text{-loop}}$ and $v_{S,1\text{-loop}}$ are the one-loop level minima, T_C in the PRM tends to be lower than that in the ordinary case, which can increase v_C/T_C . As for the determination of v_C in the PRM scheme, on the other hand, the HT potential (76) is used to maintain the gauge invariance.

Here we remark the thermal resummation in the PRM scheme. While the resummation can be implemented in a gauge-invariant way [145], it needs the two-loop effective potential $V_2(\varphi; \xi)$ for the consistency of the calculation. Nevertheless, such a calculation is not available in the literature and hence beyond the scope of this review article.

4.4. Comparisons among Various Calculation Schemes

Now we conduct numerical analysis [56]. Among the three input parameters $\{m_S, \lambda_{HS}, \lambda_S\}$, we take $m_S = m_h/2$, which is consistent with DM physics [146,147], and $\lambda_S = \lambda_S^{\text{min}} + 0.1$ [37], where λ_S^{min} is determined by the vacuum condition given in Equation (67). λ_{HS} is taken as the varying parameter. In Figure 3, numerical results of EWPT in rSM are summarized. In order to see the gauge and scale dependences on EWPT, we consider four calculation methods: the OS-like and $\overline{\text{MS}}$ schemes as the gauge-dependent methods while PRM and HT as the gauge-independent ones. In the left panel, T_C is shown as a function of λ_{HS} . As for the PRM and $\overline{\text{MS}}$ schemes, we take $m_t/2 \leq \bar{\mu} \leq 2m_t$. One can see that all the results show the same behavior, namely, T_C gets decreased as λ_{HS} increases, which is the fact that the larger λ_{HS} make the vacuum energy of I phase lower so that the degeneracy with that of EW phase happen at lower temperature. As seen, OS-like and $\overline{\text{MS}}$ schemes agree with each other nicely, while the other two gauge-invariant methods give lower T_C to some extent. For PRM, this behavior is the expected consequence as discussed above. The reason why the $\bar{\mu}$ dependence in PRM is larger than that in the $\overline{\text{MS}}$ scheme is that the one-loop minimization condition is used in the latter case, which can partially cancel the $\bar{\mu}$ dependence in determining T_C , while such a cancellation is missing due to use of the tree-level minimization condition in the former case [56].

In the right panel, v_C/T_C are plotted in the four cases. The color schemes are the same as in the left plot. The OS-like and $\overline{\text{MS}}$ schemes are consistent with each other within the scale uncertainties. On the other hand, the PRM scheme show the rather large scale uncertainties. As seen, v_C becomes zero for $\lambda_{HS} \gtrsim 0.25$, which is due to the fact that T_C in PRM gets larger than that in the HT scheme as shown in the left plot. Although somewhat big discrepancy exists among the gauge-dependent and independent schemes, we expect that it gets ameliorated when the higher-order corrections such as the daisy resummation as well as the two-loop corrections are incorporated in the PRM scheme.

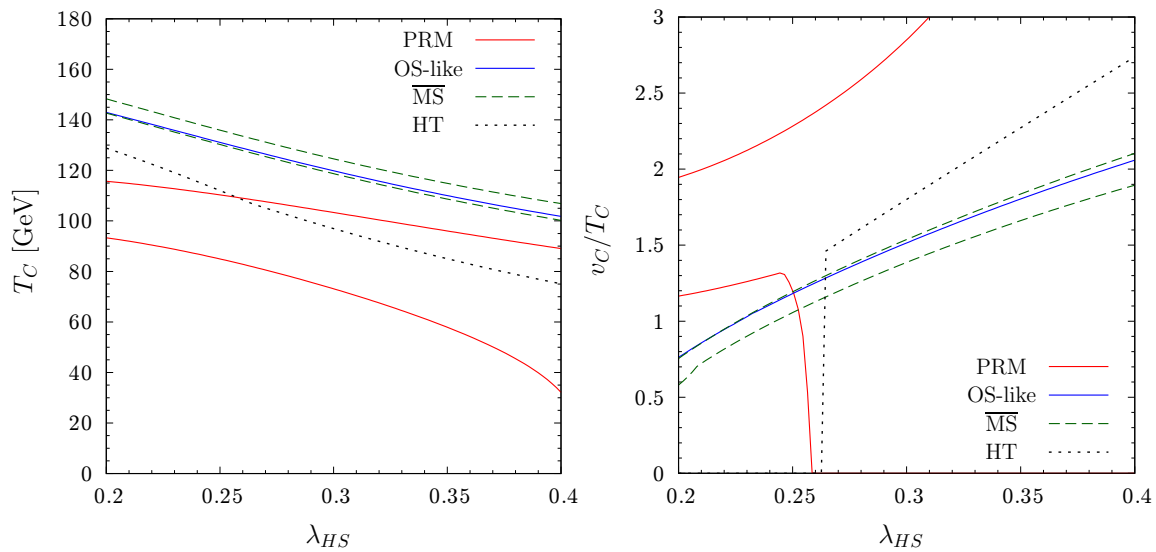


Figure 3. Comparisons among the four calculation schemes. The OS-like and \overline{MS} schemes are gauge-dependent while the PRM and HT schemes are gauge independent. For the PRM and \overline{MS} schemes, we take $m_t/2 \leq \bar{\mu} \leq 2m_t$. We take $m_S = m_h/2$ and $\lambda_S = \lambda_S^{\min} + 0.1$, where λ_S^{\min} is determined by the vacuum condition. The plots are taken from Ref. [56].

5. Summary and Outlook

We have discussed the high temperature behaviors of symmetries using the perturbative effective potential. As explicitly demonstrated in the ϕ^4 theory, the symmetry restoration generically causes the IR divergence problem that invalidates the ordinary perturbative expansion at zero temperature. To cure this problem, the dominant temperature corrections must be resummed in a consistent way. In this review, we introduce the two common methods of the thermal resummations, i.e., Parwani and Arnold-Espinosa schemes. In the former all the Matsubara frequency modes are resummed while in the latter only zero mode is resummed.

As an interesting cosmological application, we discussed EWPT focusing on the first-order phase transition case, which is motivated by EWBG as well as physics of gravitational waves. For illustration, the real scalar extended SM with the Z_2 symmetry is considered. In this model, the breaking of the Z_2 symmetry at finite temperature can increase the possibility of the first-order EWPT and its restoration at zero temperature plays a fundamental role in accommodating the DM candidate.

We also addressed the problem of gauge and scheme dependences of EWPT. The comparison is made among the four calculation methods: \overline{MS} , OS-like, PRM and HT schemes. In any case, the numerical study shows that the behaviors of the critical temperature against the coupling between the SM Higgs and real scalar are consistent with each other and indicates the occurrence of the first-order EWPT (for the PRM scheme within the scale uncertainties). Nevertheless, none of the methods are gauge invariant and less scale dependent, which motivates one to refine the calculations including higher-order corrections.

In closing, through the demonstration here, we highlight the technical issues of the perturbative treatments of the thermal phase transition and illustrate the need to exercise caution when applying them to EWPT. However, this does not necessarily mean that the issues are just technical. In the current perturbative approach, for instance, the order parameter is the VEV of the Higgs field which is inherently gauge dependent. We may need to find better order parameter and newly develop formalism rather than fixing the drawbacks of the current methods.

Funding: This research received no external funding.

Acknowledgments: I would like to thank all my collaborators for fruitful discussions.

Conflicts of Interest: The author declares no conflict of interest.

Appendix A. Thermally Corrected Field-Dependent Masses in the rSM

The thermally corrected Higgs mass matrix takes the form

$$\bar{\mathcal{M}}_H^2 = \begin{pmatrix} -\mu_H^2 + 3\lambda_H\varphi^2 + \frac{\lambda_{HS}}{2}\varphi_S^2 + \Sigma_H(T) & \lambda_{HS}\varphi\varphi_S \\ \lambda_{HS}\varphi\varphi_S & -\mu_S^2 + 3\lambda_S\varphi_S^2 + \frac{\lambda_{HS}}{2}\varphi^2 + \Sigma_S(T) \end{pmatrix}, \quad (\text{A1})$$

where $\Sigma_H(T)$ and $\Sigma_S(T)$ are given by Equations (69) and (70). For the NG bosons, one finds

$$\bar{M}_{G^0}^2 = \bar{M}_{G^\pm}^2 = -\mu_H^2 + \lambda_H\varphi^2 + \frac{\lambda_{HS}}{2}\varphi_S^2 + \Sigma_H(T). \quad (\text{A2})$$

As given in Equation (33), there are two distinct thermal masses for the longitudinal and transverse gauge fields. At one-loop order, only the former receive the nonzero corrections. The thermally corrected gauge boson mass matrix in the basis $(A_\mu^1, A_\mu^2, A_\mu^3, B_\mu)$ is cast into the form

$$\bar{\mathcal{M}}_{V_L}^2 = \begin{pmatrix} g_2^2\varphi^2/4 + \Pi_W(T) & 0 & 0 & 0 \\ 0 & g_2^2\varphi^2/4 + \Pi_W(T) & 0 & 0 \\ 0 & 0 & g_2^2\varphi^2/4 + \Pi_W(T) & -g_2g_1\varphi^2/4 \\ 0 & 0 & -g_2g_1\varphi^2/4 & g_1^2\varphi^2/4 + \Pi_B(T) \end{pmatrix}. \quad (\text{A3})$$

The corresponding eigenvalues are, respectively, given by

$$\bar{M}_{Z_L, \gamma_L}^2 = \frac{1}{2} \left[\frac{1}{4}(g_2^2 + g_1^2)\varphi^2 + \Pi_W(T) + \Pi_B(T) \pm \sqrt{\left(\frac{1}{4}(g_2^2 - g_1^2)\varphi^2 + \Pi_W(T) - \Pi_B(T) \right)^2 + \frac{g_2^2g_1^2}{4}\varphi^4} \right], \quad (\text{A4})$$

$$\bar{M}_{W_L}^2 = \bar{m}_W^2 + \Pi_W(T), \quad (\text{A5})$$

where $\Pi_W(T)$ and $\Pi_B(T)$ are [148]

$$\Pi_W(T) = \left[\frac{5}{6} + \frac{N_g(N_C + 1)}{12} \right] g_2^2 T^2 \Big|_{N_g=N_C=3} = \frac{11}{6} g_2^2 T^2, \quad (\text{A6})$$

$$\Pi_B(T) = \left[\frac{1}{6} + \frac{N_g}{12} \left(\frac{11}{9} N_C + 3 \right) \right] g_1^2 T^2 \Big|_{N_g=N_C=3} = \frac{11}{6} g_1^2 T^2. \quad (\text{A7})$$

where N_g denotes the number of fermion generation and N_C is the number of color, and the last equalities are evaluated with $N_g = N_C = 3$.

References

1. Kirzhnits, D.A. Weinberg model in the hot universe. *JETP Lett.* **1972**, *15*, 529–531.
2. Kirzhnits, D.A.; Linde, A.D. Macroscopic Consequences of the Weinberg Model. *Phys. Lett.* **1972**, *42B*, 471–474. [[CrossRef](#)]
3. Dolan, L.; Jackiw, R. Symmetry Behavior at Finite Temperature. *Phys. Rev.* **1974**, *D9*, 3320–3341. [[CrossRef](#)]
4. Weinberg, S. Gauge and Global Symmetries at High Temperature. *Phys. Rev.* **1974**, *D9*, 3357–3378. [[CrossRef](#)]
5. Kirzhnits, D.A.; Linde, A.D. Symmetry Behavior in Gauge Theories. *Ann. Phys.* **1976**, *101*, 195–238. [[CrossRef](#)]
6. Particle Data Group. Review of Particle Physics. *Phys. Rev.* **2018**, *D98*, 030001. [[CrossRef](#)]
7. Kuzmin, V.A.; Rubakov, V.A.; Shaposhnikov, M.E. On the Anomalous Electroweak Baryon Number Nonconservation in the Early Universe. *Phys. Lett.* **1985**, *155B*, 36. [[CrossRef](#)]
8. Rubakov, V.A.; Shaposhnikov, M.E. Electroweak baryon number nonconservation in the early universe and in high-energy collisions. *Usp. Fiz. Nauk* **1996**, *166*, 493–537. [[CrossRef](#)]

9. Funakubo, K. CP violation and baryogenesis at the electroweak phase transition. *Prog. Theor. Phys.* **1996**, *96*, 475–520. [[CrossRef](#)]
10. Riotto, A. Theories of baryogenesis. In Proceedings of the Summer School in High-energy physics and cosmology, Trieste, Italy, 29 June–17 July 1998; pp. 326–436.
11. Quiros, M. Finite temperature field theory and phase transitions. In Proceedings of the Summer School in High-Energy Physics and Cosmology, Trieste, Italy, 29 June–17 July 1998; pp. 187–259.
12. Trodden, M. Electroweak baryogenesis. *Rev. Mod. Phys.* **1999**, *71*, 1463–1500. [[CrossRef](#)]
13. Bernreuther, W. CP violation and baryogenesis. *Lect. Notes Phys.* **2002**, *591*, 237–293.
14. Cline, J.M. Baryogenesis. In Proceedings of the Les Houches Summer School - Session 86: Particle Physics and Cosmology: The Fabric of Spacetime Les Houches, Les Houches, France, 31 July–25 August 2006.
15. Morrissey, D.E.; Ramsey-Musolf, M.J. Electroweak baryogenesis. *New J. Phys.* **2012**, *14*, 125003. [[CrossRef](#)]
16. Konstandin, T. Quantum Transport and Electroweak Baryogenesis. *Phys. Usp.* **2013**, *56*, 747–771. [[CrossRef](#)]
17. Caprini, C.; Hindmarsh, M.; Huber, S.; Konstandin, T.; Kozaczuk, J.; Nardini, G.; No, J.M.; Petiteau, A.; Schwaller, P.; Servant, G.; et al. Science with the space-based interferometer eLISA. II: Gravitational waves from cosmological phase transitions. *JCAP* **2016**, *1604*, 001. [[CrossRef](#)]
18. Choi, J.; Volkas, R.R. Real Higgs singlet and the electroweak phase transition in the Standard Model. *Phys. Lett.* **1993**, *B317*, 385–391. [[CrossRef](#)]
19. Ham, S.W.; Jeong, Y.S.; Oh, S.K. Electroweak phase transition in an extension of the standard model with a real Higgs singlet. *J. Phys.* **2005**, *G31*, 857–871. [[CrossRef](#)]
20. Ahriche, A. What is the criterion for a strong first order electroweak phase transition in singlet models? *Phys. Rev.* **2007**, *D75*, 083522. [[CrossRef](#)]
21. Espinosa, J.R.; Quiros, M. Novel Effects in Electroweak Breaking from a Hidden Sector. *Phys. Rev.* **2007**, *D76*, 076004. [[CrossRef](#)]
22. Das, S.; Fox, P.J.; Kumar, A.; Weiner, N. The Dark Side of the Electroweak Phase Transition. *JHEP* **2010**, *11*, 108. [[CrossRef](#)]
23. Chung, D.J.H.; Long, A.J. Cosmological Constant, Dark Matter, and Electroweak Phase Transition. *Phys. Rev.* **2011**, *D84*, 103513. [[CrossRef](#)]
24. Espinosa, J.R.; Gripiaios, B.; Konstandin, T.; Riva, F. Electroweak Baryogenesis in Non-minimal Composite Higgs Models. *JCAP* **2012**, *1201*, 012. [[CrossRef](#)]
25. Cline, J.M.; Kainulainen, K. Electroweak baryogenesis and dark matter from a singlet Higgs. *JCAP* **2013**, *1301*, 012. [[CrossRef](#)]
26. Fairbairn, M.; Hogan, R. Singlet Fermionic Dark Matter and the Electroweak Phase Transition. *JHEP* **2013**, *09*, 022. [[CrossRef](#)]
27. Cline, J.M.; Kainulainen, K.; Scott, P.; Weniger, C. Update on scalar singlet dark matter. *Phys. Rev.* **2013**, *D88*, 055025. [[CrossRef](#)]
28. Damgaard, P.H.; O'Connell, D.; Petersen, T.C.; Tranberg, A. Constraints on New Physics from Baryogenesis and Large Hadron Collider Data. *Phys. Rev. Lett.* **2013**, *111*, 221804. [[CrossRef](#)]
29. Li, T.; Zhou, Y.F. Strongly first order phase transition in the singlet fermionic dark matter model after LUX. *JHEP* **2014**, *07*, 006. [[CrossRef](#)]
30. Profumo, S.; Ramsey-Musolf, M.J.; Shaughnessy, G. Singlet Higgs phenomenology and the electroweak phase transition. *JHEP* **2007**, *08*, 010. [[CrossRef](#)]
31. Ashoorioon, A.; Konstandin, T. Strong electroweak phase transitions without collider traces. *JHEP* **2009**, *07*, 086. [[CrossRef](#)]
32. Espinosa, J.R.; Konstandin, T.; Riva, F. Strong Electroweak Phase Transitions in the Standard Model with a Singlet. *Nucl. Phys.* **2012**, *B854*, 592–630. [[CrossRef](#)]
33. Fuyuto, K.; Senaha, E. Improved sphaleron decoupling condition and the Higgs coupling constants in the real singlet-extended standard model. *Phys. Rev.* **2014**, *D90*, 015015. [[CrossRef](#)]
34. Alanne, T.; Tuominen, K.; Vaskonen, V. Strong phase transition, dark matter and vacuum stability from simple hidden sectors. *Nucl. Phys.* **2014**, *B889*, 692–711. [[CrossRef](#)]
35. Profumo, S.; Ramsey-Musolf, M.J.; Wainwright, C.L.; Winslow, P. Singlet-catalyzed electroweak phase transitions and precision Higgs boson studies. *Phys. Rev.* **2015**, *D91*, 035018. [[CrossRef](#)]
36. Craig, N.; Lou, H.K.; McCullough, M.; Thalappilil, A. The Higgs Portal Above Threshold. *JHEP* **2016**, *02*, 127. [[CrossRef](#)]

37. Curtin, D.; Meade, P.; Yu, C.T. Testing Electroweak Baryogenesis with Future Colliders. *JHEP* **2014**, *11*, 127. [[CrossRef](#)]
38. Kozaczuk, J. Bubble Expansion and the Viability of Singlet-Driven Electroweak Baryogenesis. *JHEP* **2015**, *10*, 135. [[CrossRef](#)]
39. Damgaard, P.H.; Haarr, A.; O'Connell, D.; Tranberg, A. Effective Field Theory and Electroweak Baryogenesis in the Singlet-Extended Standard Model. *JHEP* **2016**, *02*, 107. [[CrossRef](#)]
40. Ghosh, S.; Kundu, A.; Ray, S. Potential of a singlet scalar enhanced Standard Model. *Phys. Rev.* **2016**, *D93*, 115034. [[CrossRef](#)]
41. Kotwal, A.V.; Ramsey-Musolf, M.J.; No, J.M.; Winslow, P. Singlet-catalyzed electroweak phase transitions in the 100 TeV frontier. *Phys. Rev.* **2016**, *D94*, 035022. [[CrossRef](#)]
42. Chala, M.; Nardini, G.; Sobolev, I. Unified explanation for dark matter and electroweak baryogenesis with direct detection and gravitational wave signatures. *Phys. Rev.* **2016**, *D94*, 055006. [[CrossRef](#)]
43. Tenkanen, T.; Tuominen, K.; Vaskonen, V. A Strong Electroweak Phase Transition from the Inflaton Field. *JCAP* **2016**, *1609*, 037. [[CrossRef](#)]
44. Huang, P.; Long, A.J.; Wang, L.T. Probing the Electroweak Phase Transition with Higgs Factories and Gravitational Waves. *Phys. Rev.* **2016**, *D94*, 075008. [[CrossRef](#)]
45. Vaskonen, V. Electroweak baryogenesis and gravitational waves from a real scalar singlet. *Phys. Rev.* **2017**, *D95*, 123515. [[CrossRef](#)]
46. Curtin, D.; Meade, P.; Ramani, H. Thermal Resummation and Phase Transitions. *Eur. Phys. J.* **2018**, *C78*, 787. [[CrossRef](#)]
47. Cline, J.M.; Kainulainen, K.; Tucker-Smith, D. Electroweak baryogenesis from a dark sector. *Phys. Rev.* **2017**, *D95*, 115006. [[CrossRef](#)]
48. Beniwal, A.; Lewicki, M.; Wells, J.D.; White, M.; Williams, A.G. Gravitational wave, collider and dark matter signals from a scalar singlet electroweak baryogenesis. *JHEP* **2017**, *08*, 108. [[CrossRef](#)]
49. Ghorbani, P.H. Electroweak Baryogenesis and Dark Matter via a Pseudoscalar vs. Scalar. *JHEP* **2017**, *08*, 058. [[CrossRef](#)]
50. Marzola, L.; Racioppi, A.; Vaskonen, V. Phase transition and gravitational wave phenomenology of scalar conformal extensions of the Standard Model. *Eur. Phys. J.* **2017**, *C77*, 484. [[CrossRef](#)]
51. Chen, C.Y.; Kozaczuk, J.; Lewis, I.M. Non-resonant Collider Signatures of a Singlet-Driven Electroweak Phase Transition. *JHEP* **2017**, *08*, 096. [[CrossRef](#)]
52. Kurup, G.; Perelstein, M. Dynamics of Electroweak Phase Transition In Singlet-Scalar Extension of the Standard Model. *Phys. Rev.* **2017**, *D96*, 015036. [[CrossRef](#)]
53. Jain, B.; Lee, S.J.; Son, M. Validity of the effective potential and the precision of Higgs field self-couplings. *Phys. Rev.* **2018**, *D98*, 075002. [[CrossRef](#)]
54. Ghorbani, K.; Ghorbani, P.H. Strongly First-Order Phase Transition in Real Singlet Scalar Dark Matter Model. *J. Phys.* **2020**, *G47*, 015201. [[CrossRef](#)]
55. Huang, F.P.; Qian, Z.; Zhang, M. Exploring dynamical CP violation induced baryogenesis by gravitational waves and colliders. *Phys. Rev.* **2018**, *D98*, 015014. [[CrossRef](#)]
56. Chiang, C.W.; Li, Y.T.; Senaha, E. Revisiting electroweak phase transition in the standard model with a real singlet scalar. *Phys. Lett.* **2019**, *B789*, 154–159. [[CrossRef](#)]
57. Beniwal, A.; Lewicki, M.; White, M.; Williams, A.G. Gravitational waves and electroweak baryogenesis in a global study of the extended scalar singlet model. *JHEP* **2019**, *02*, 183. [[CrossRef](#)]
58. Carena, M.; Liu, Z.; Wang, Y. Electroweak Phase Transition with Spontaneous Z_2 -Breaking. 2019. Available online: <http://xxx.lanl.gov/abs/1911.10206> (accessed on 20 April 2020).
59. Kondo, Y.; Umemura, I.; Yamamoto, K. First order phase transition in the singlet Majoron model. *Phys. Lett.* **1991**, *B263*, 93–96. [[CrossRef](#)]
60. Espinosa, J.R.; Quiros, M. The Electroweak phase transition with a singlet. *Phys. Lett.* **1993**, *B305*, 98–105. [[CrossRef](#)]
61. Benson, K.E.C. Avoiding baryon washout in the extended Standard Model. *Phys. Rev.* **1993**, *D48*, 2456–2461. [[CrossRef](#)]
62. Cline, J.M.; Laporte, G.; Yamashita, H.; Kraml, S. Electroweak Phase Transition and LHC Signatures in the Singlet Majoron Model. *JHEP* **2009**, *07*, 040. [[CrossRef](#)]

63. Farzinnia, A.; Ren, J. Strongly First-Order Electroweak Phase Transition and Classical Scale Invariance. *Phys. Rev.* **2014**, *D90*, 075012. [[CrossRef](#)]
64. Chao, W. First order electroweak phase transition triggered by the Higgs portal vector dark matter. *Phys. Rev.* **2015**, *D92*, 015025. [[CrossRef](#)]
65. Kang, Z.; Ko, P.; Matsui, T. Strong first order EWPT & strong gravitational waves in Z_3 -symmetric singlet scalar extension. *JHEP* **2018**, *02*, 115. [[CrossRef](#)]
66. Chiang, C.W.; Ramsey-Musolf, M.J.; Senaha, E. Standard Model with a Complex Scalar Singlet: Cosmological Implications and Theoretical Considerations. *Phys. Rev.* **2018**, *D97*, 015005. [[CrossRef](#)]
67. Cheng, W.; Bian, L. From inflation to cosmological electroweak phase transition with a complex scalar singlet. *Phys. Rev.* **2018**, *D98*, 023524. [[CrossRef](#)]
68. Grzadkowski, B.; Huang, D. Spontaneous CP-Violating Electroweak Baryogenesis and Dark Matter from a Complex Singlet Scalar. *JHEP* **2018**, *08*, 135. [[CrossRef](#)]
69. Chen, N.; Li, T.; Wu, Y.; Bian, L. Discriminate the Discrete Symmetry Through the Future e^+e^- Colliders and Gravitational Waves. 2019. Available online: <http://xxx.lanl.gov/abs/1911.05579> (accessed on 20 April 2020).
70. Bochkarev, A.I.; Kuzmin, S.V.; Shaposhnikov, M.E. Electroweak baryogenesis and the Higgs boson mass problem. *Phys. Lett.* **1990**, *B244*, 275–278. [[CrossRef](#)]
71. Turok, N.; Zadrozny, J. Phase transitions in the two doublet model. *Nucl. Phys.* **1992**, *B369*, 729–742. [[CrossRef](#)]
72. Land, D.; Carlson, E.D. Two stage phase transition in two Higgs models. *Phys. Lett.* **1992**, *B292*, 107–112. [[CrossRef](#)]
73. Hammerschmitt, A.; Kripfganz, J.; Schmidt, M.G. Baryon asymmetry from a two stage electroweak phase transition? *Z. Phys.* **1994**, *C64*, 105–110. [[CrossRef](#)]
74. Funakubo, K.; Kakuto, A.; Takenaga, K. The Effective potential of electroweak theory with two massless Higgs doublets at finite temperature. *Prog. Theor. Phys.* **1994**, *91*, 341–352. [[CrossRef](#)]
75. Cline, J.M.; Lemieux, P.A. Electroweak phase transition in two Higgs doublet models. *Phys. Rev.* **1997**, *D55*, 3873–3881. [[CrossRef](#)]
76. Kanemura, S.; Okada, Y.; Senaha, E. Electroweak baryogenesis and quantum corrections to the triple Higgs boson coupling. *Phys. Lett.* **2005**, *B606*, 361–366. [[CrossRef](#)]
77. Fromme, L.; Huber, S.J.; Seniuch, M. Baryogenesis in the two-Higgs doublet model. *JHEP* **2006**, *11*, 038. [[CrossRef](#)]
78. Chowdhury, T.A.; Nemevsek, M.; Senjanovic, G.; Zhang, Y. Dark Matter as the Trigger of Strong Electroweak Phase Transition. *JCAP* **2012**, *1202*, 029. [[CrossRef](#)]
79. Borah, D.; Cline, J.M. Inert Doublet Dark Matter with Strong Electroweak Phase Transition. *Phys. Rev.* **2012**, *D86*, 055001. [[CrossRef](#)]
80. Gil, G.; Chankowski, P.; Krawczyk, M. Inert Dark Matter and Strong Electroweak Phase Transition. *Phys. Lett.* **2012**, *B717*, 396–402. [[CrossRef](#)]
81. Cline, J.M.; Kainulainen, K. Improved Electroweak Phase Transition with Subdominant Inert Doublet Dark Matter. *Phys. Rev.* **2013**, *D87*, 071701. [[CrossRef](#)]
82. Dorsch, G.C.; Huber, S.J.; No, J.M. A strong electroweak phase transition in the 2HDM after LHC8. *JHEP* **2013**, *10*, 029. [[CrossRef](#)]
83. Dorsch, G.C.; Huber, S.J.; Mimasu, K.; No, J.M. Echoes of the Electroweak Phase Transition: Discovering a second Higgs doublet through $A_0 \rightarrow ZH_0$. *Phys. Rev. Lett.* **2014**, *113*, 211802. [[CrossRef](#)]
84. Blinov, N.; Profumo, S.; Stefaniak, T. The Electroweak Phase Transition in the Inert Doublet Model. *JCAP* **2015**, *1507*, 028. [[CrossRef](#)]
85. Fuyuto, K.; Senaha, E. Sphaleron and critical bubble in the scale invariant two Higgs doublet model. *Phys. Lett.* **2015**, *B747*, 152–157. [[CrossRef](#)]
86. Basler, P.; Mühlleitner, M.; Wittbrodt, J. The CP-Violating 2HDM in Light of a Strong First Order Electroweak Phase Transition and Implications for Higgs Pair Production. *JHEP* **2018**, *03*, 061. [[CrossRef](#)]
87. Huang, F.P.; Senaha, E. Enhanced Z boson decays as a new probe of first-order electroweak phase transition at future lepton colliders. *Phys. Rev.* **2019**, *D100*, 035014. [[CrossRef](#)]
88. Wang, X.; Huang, F.P.; Zhang, X. Gravitational wave and collider signals in complex two-Higgs doublet model with dynamical CP-violation at finite temperature. *Phys. Rev.* **2020**, *D101*, 015015. [[CrossRef](#)]

89. Pietroni, M. The Electroweak phase transition in a nonminimal supersymmetric model. *Nucl. Phys.* **1993**, *B402*, 27–45. [[CrossRef](#)]
90. Espinosa, J.R.; Quiros, M.; Zwirner, F. On the electroweak phase transition in the minimal supersymmetric Standard Model. *Phys. Lett.* **1993**, *B307*, 106–115. [[CrossRef](#)]
91. Brignole, A.; Espinosa, J.R.; Quiros, M.; Zwirner, F. Aspects of the electroweak phase transition in the minimal supersymmetric standard model. *Phys. Lett.* **1994**, *B324*, 181–191. [[CrossRef](#)]
92. Davies, A.T.; Froggatt, C.D.; Moorhouse, R.G. Electroweak baryogenesis in the next-to-minimal supersymmetric model. *Phys. Lett.* **1996**, *B372*, 88–94. [[CrossRef](#)]
93. Espinosa, J.R. Dominant two loop corrections to the MSSM finite temperature effective potential. *Nucl. Phys.* **1996**, *B475*, 273–292. [[CrossRef](#)]
94. De Carlos, B.; Espinosa, J.R. The Baryogenesis window in the MSSM. *Nucl. Phys.* **1997**, *B503*, 24–54. [[CrossRef](#)]
95. Huber, S.J.; Schmidt, M.G. Electroweak baryogenesis: Concrete in a SUSY model with a gauge singlet. *Nucl. Phys.* **2001**, *B606*, 183–230. [[CrossRef](#)]
96. Funakubo, K.; Tao, S.; Toyoda, F. CP violation in the Higgs sector and phase transition in the MSSM. *Prog. Theor. Phys.* **2003**, *109*, 415–432. [[CrossRef](#)]
97. Funakubo, K.; Tao, S.; Toyoda, F. Phase transitions in the NMSSM. *Prog. Theor. Phys.* **2005**, *114*, 369–389. [[CrossRef](#)]
98. Huber, S.J.; Konstandin, T.; Prokopec, T.; Schmidt, M.G. Electroweak Phase Transition and Baryogenesis in the nMSSM. *Nucl. Phys.* **2006**, *B757*, 172–196. [[CrossRef](#)]
99. Funakubo, K.; Senaha, E. Electroweak phase transition, critical bubbles and sphaleron decoupling condition in the MSSM. *Phys. Rev.* **2009**, *D79*, 115024. [[CrossRef](#)]
100. Chiang, C.W.; Senaha, E. Electroweak phase transitions in the secluded U(1)-prime-extended MSSM. *JHEP* **2010**, *06*, 030. [[CrossRef](#)]
101. Chung, D.J.H.; Long, A.J. Electroweak Phase Transition in the mnuSSM. *Phys. Rev.* **2010**, *D81*, 123531. [[CrossRef](#)]
102. Kanemura, S.; Senaha, E.; Shindou, T. First-order electroweak phase transition powered by additional F-term loop effects in an extended supersymmetric Higgs sector. *Phys. Lett.* **2011**, *B706*, 40–45. [[CrossRef](#)]
103. Carena, M.; Shah, N.R.; Wagner, C.E.M. Light Dark Matter and the Electroweak Phase Transition in the NMSSM. *Phys. Rev.* **2012**, *D85*, 036003. [[CrossRef](#)]
104. Fok, R.; Kribs, G.D.; Martin, A.; Tsai, Y. Electroweak Baryogenesis in R-symmetric Supersymmetry. *Phys. Rev.* **2013**, *D87*, 055018. [[CrossRef](#)]
105. Kanemura, S.; Senaha, E.; Shindou, T.; Yamada, T. Electroweak phase transition and Higgs boson couplings in the model based on supersymmetric strong dynamics. *JHEP* **2013**, *05*, 066. [[CrossRef](#)]
106. Kozaczuk, J.; Profumo, S.; Haskins, L.S.; Wainwright, C.L. Cosmological Phase Transitions and their Properties in the NMSSM. *JHEP* **2015**, *01*, 144. [[CrossRef](#)]
107. Athron, P.; Balazs, C.; Fowlie, A.; Pozzo, G.; White, G.; Zhang, Y. Strong first-order phase transitions in the NMSSM—A comprehensive survey. *JHEP* **2019**, *11*, 151. [[CrossRef](#)]
108. Linde, A.D. Infrared Problem in Thermodynamics of the Yang-Mills Gas. *Phys. Lett.* **1980**, *96B*, 289–292. [[CrossRef](#)]
109. Nielsen, N.K. On the Gauge Dependence of Spontaneous Symmetry Breaking in Gauge Theories. *Nucl. Phys.* **1975**, *B101*, 173–188. [[CrossRef](#)]
110. Fukuda, R.; Kugo, T. Gauge Invariance in the Effective Action and Potential. *Phys. Rev.* **1976**, *D13*, 3469. [[CrossRef](#)]
111. Jackiw, R. Functional evaluation of the effective potential. *Phys. Rev.* **1974**, *D9*, 1686. [[CrossRef](#)]
112. Coleman, S.R.; Weinberg, E.J. Radiative Corrections as the Origin of Spontaneous Symmetry Breaking. *Phys. Rev.* **1973**, *D7*, 1888–1910. [[CrossRef](#)]
113. Weinberg, E.J.; Wu, A.Q. Understanding Complex Perturbative Effective Potentials. *Phys. Rev. D* **1987**, *36*, 2474. [[CrossRef](#)]
114. Mazumdar, A.; White, G. Review of cosmic phase transitions: Their significance and experimental signatures. *Rept. Prog. Phys.* **2019**, *82*, 076901. [[CrossRef](#)]
115. Espinosa, J.R.; Quiros, M.; Zwirner, F. On the phase transition in the scalar theory. *Phys. Lett.* **1992**, *B291*, 115–124. [[CrossRef](#)]

116. Arnold, P.B.; Espinosa, O. The Effective potential and first order phase transitions: Beyond leading-order. *Phys. Rev.* **1993**, *D47*, 3546. [[CrossRef](#)] [[PubMed](#)]
117. Amelino-Camelia, G.; Pi, S.Y. Selfconsistent improvement of the finite temperature effective potential. *Phys. Rev.* **1993**, *D47*, 2356–2362. [[CrossRef](#)]
118. Parwani, R.R. Resummation in a hot scalar field theory. *Phys. Rev.* **1992**, *D45*, 4695. [[CrossRef](#)] [[PubMed](#)]
119. Kainulainen, K.; Keus, V.; Niemi, L.; Rummukainen, K.; Tenkanen, T.V.I.; Vaskonen, V. On the validity of perturbative studies of the electroweak phase transition in the Two Higgs Doublet model. *JHEP* **2019**, *06*, 075. [[CrossRef](#)]
120. Peskin, M.E.; Schroeder, D.V. *An Introduction to Quantum Field Theory*; Addison-Wesley: Reading, PA, USA, 1995.
121. Takahashi, K. Perturbative Calculations at Finite Temperatures. *Z. Phys.* **1985**, *C26*, 601–613. [[CrossRef](#)]
122. Arafune, J.; Ogure, K.; Sato, J. Nonperturbative evaluation of the effective potential of $\lambda\phi^4$ theory at finite temperature under the superdaisy approximation. *Prog. Theor. Phys.* **1998**, *99*, 119–128. [[CrossRef](#)]
123. Inagaki, T.; Ogure, K.; Sato, J. Nonperturbative approach to the effective potential of the $\lambda\phi^4$ theory at finite temperature. *Prog. Theor. Phys.* **1998**, *99*, 1069–1084. [[CrossRef](#)]
124. Smet, G.; Vanzielighem, T.; Van Acoleyen, K.; Verschelde, H. A 2 loop 2PPI analysis of $\lambda\phi^4$ at finite temperature. *Phys. Rev.* **2002**, *D65*, 045015. [[CrossRef](#)]
125. Marko, G.; Reinoso, U.; Szep, Z. Broken Phase Effective Potential in the Two-Loop Phi-Derivable Approximation and Nature of the Phase Transition in a Scalar Theory. *Phys. Rev.* **2012**, *D86*, 085031. [[CrossRef](#)]
126. Bellac, M.L. *Thermal Field Theory*; Cambridge Monographs on Mathematical Physics, Cambridge University Press: Cambridge, UK, 2011. [[CrossRef](#)]
127. Gross, D.J.; Pisarski, R.D.; Yaffe, L.G. QCD and Instantons at Finite Temperature. *Rev. Mod. Phys.* **1981**, *53*, 43. [[CrossRef](#)]
128. Frenkel, J.; Taylor, J.C. High Temperature Limit of Thermal QCD. *Nucl. Phys.* **1990**, *B334*, 199–216. [[CrossRef](#)]
129. Braaten, E.; Pisarski, R.D. Resummation and Gauge Invariance of the Gluon Damping Rate in Hot QCD. *Phys. Rev. Lett.* **1990**, *64*, 1338. [[CrossRef](#)] [[PubMed](#)]
130. Braaten, E.; Pisarski, R.D. Soft Amplitudes in Hot Gauge Theories: A General Analysis. *Nucl. Phys.* **1990**, *B337*, 569–634. [[CrossRef](#)]
131. Braaten, E.; Pisarski, R.D. Simple effective Lagrangian for hard thermal loops. *Phys. Rev.* **1992**, *D45*, R1827. [[CrossRef](#)] [[PubMed](#)]
132. Blaizot, J.P.; Iancu, E. The Quark gluon plasma: Collective dynamics and hard thermal loops. *Phys. Rept.* **2002**, *359*, 355–528. [[CrossRef](#)]
133. Kraemmer, U.; Rebhan, A. Advances in perturbative thermal field theory. *Rept. Prog. Phys.* **2004**, *67*, 351. [[CrossRef](#)]
134. Hofmann, R. Nonperturbative approach to Yang-Mills thermodynamics. *Int. J. Mod. Phys.* **2005**, *A20*, 4123–4216. [[CrossRef](#)]
135. Kapusta, J.I.; Gale, C. *Finite-Temperature Field Theory: Principles and Applications*; Cambridge Monographs on Mathematical Physics, Cambridge University Press: Cambridge, UK, 2011. [[CrossRef](#)]
136. Bischer, I.; Grandou, T.; Hofmann, R. On Quantum Fields at High Temperature. *Universe* **2019**, *5*, 26. [[CrossRef](#)]
137. Fujii, K.; Grojean, C.; Peskin, M.E.; Barklow, T.; Gao, Y.; Kanemura, S.; Kim, H.; List, J.; Nojiri, M.; Perelstein, M.; et al. Physics Case for the International Linear Collider. 2015. Available online: <http://xxx.lanl.gov/abs/1506.05992>. (accessed on 20 April 2020).
138. Gonçalves, D.; Han, T.; Kling, F.; Plehn, T.; Takeuchi, M. Higgs boson pair production at future hadron colliders: From kinematics to dynamics. *Phys. Rev.* **2018**, *D97*, 113004. [[CrossRef](#)]
139. Chang, J.; Cheung, K.; Lee, J.S.; Lu, C.T.; Park, J. Higgs-boson-pair production $H(\rightarrow b\bar{b})H(\rightarrow \gamma\gamma)$ from gluon fusion at the HL-LHC and HL-100 TeV hadron collider. *Phys. Rev.* **2019**, *D100*, 096001. [[CrossRef](#)]
140. Kajantie, K.; Laine, M.; Rummukainen, K.; Shaposhnikov, M.E. Is there a hot electroweak phase transition at $m(H)$ larger or equal to $m(W)$? *Phys. Rev. Lett.* **1996**, *77*, 2887–2890. [[CrossRef](#)] [[PubMed](#)]
141. Rummukainen, K.; Tsypin, M.; Kajantie, K.; Laine, M.; Shaposhnikov, M.E. The Universality class of the electroweak theory. *Nucl. Phys.* **1998**, *B532*, 283–314. [[CrossRef](#)]

142. Csikor, F.; Fodor, Z.; Heitger, J. Endpoint of the hot electroweak phase transition. *Phys. Rev. Lett.* **1999**, *82*, 21–24. [[CrossRef](#)]
143. Aoki, Y.; Csikor, F.; Fodor, Z.; Ukawa, A. The Endpoint of the first order phase transition of the SU(2) gauge Higgs model on a four-dimensional isotropic lattice. *Phys. Rev.* **1999**, *D60*, 013001. [[CrossRef](#)]
144. D’Onofrio, M.; Rummukainen, K.; Tranberg, A. Sphaleron Rate in the Minimal Standard Model. *Phys. Rev. Lett.* **2014**, *113*, 141602. [[CrossRef](#)] [[PubMed](#)]
145. Patel, H.H.; Ramsey-Musolf, M.J. Baryon Washout, Electroweak Phase Transition, and Perturbation Theory. *JHEP* **2011**, *07*, 029. [[CrossRef](#)]
146. Athron, P.; Balazs, C.; Bringmann, T.; Buckley, A.; Chruszcz, M.; Conrad, J.; Cornell, J.M.; Dal, L.A.; Edsjo, J.; Farmer, B.; et al. Status of the scalar singlet dark matter model. *Eur. Phys. J.* **2017**, *C77*, 568. [[CrossRef](#)]
147. Athron, P.; Cornell, J.M.; Kahlhoefer, F.; McKay, J.; Scott, P.; Wild, S. Impact of vacuum stability, perturbativity and XENON1T on global fits of \mathbb{Z}_2 and \mathbb{Z}_3 scalar singlet dark matter. *Eur. Phys. J.* **2018**, *C78*, 830. [[CrossRef](#)]
148. Carrington, M.E. The Effective potential at finite temperature in the Standard Model. *Phys. Rev.* **1992**, *D45*, 2933–2944. [[CrossRef](#)]



© 2020 by the author. Licensee MDPI, Basel, Switzerland. This article is an open access article distributed under the terms and conditions of the Creative Commons Attribution (CC BY) license (<http://creativecommons.org/licenses/by/4.0/>).